

**Mineralization and Ore Controls
of the Shasta Ag-Au Deposit,
Toodoggone River Area, British Columbia**

by

Peter C. Thiersch

**A thesis submitted to
the Faculty of Graduate Studies and Research
in partial fulfilment of the requirements for
the degree of Master of Science**

**Department of Earth and Planetary Sciences
McGill University, Montreal**

© Peter C. Thiersch, May 1993

Ore controls of the Shasta Ag-Au deposit, British Columbia

ABSTRACT

The Shasta AgAu deposit, located in the Toadogone River area of north-central British Columbia, has many characteristics of the low sulphidation, adularia-sericite class of epithermal deposit. It consists of quartz-calcite stockworks and breccias associated with potassic (K-feldspar+sericite) alteration of dacitic ruff host rocks. Ore grade mineralization occurs mainly in Bonanza-style breccias which host electrum, electron and native silver, associated with pyrite, sphalerite, chalcocite, galena, chlorite and hematite. However, Shasta lacks vein-hosted adularia. The highest grades of ore are associated with calcite-rich breccias, which are features atypical of the adularia-sericite class.

Hydrothermal breccias, chalcedonic quartz and abundant vapour rich fluid inclusions are strong evidence for boiling of the vein fluid. Fluid inclusion evidence indicates that ore was deposited between 280° and 225°C at a maximum depth of 750 m, from a relatively dilute hydrothermal fluid. Oxygen and hydrogen isotopic data suggest that the fluid was meteoric in origin. Initial log fO_2 , -pH conditions were estimated to have been between -33 to -31, and 4.25 to 6, respectively, and to have increased during mineralization.

A model is proposed in which quartz, and subsequently calcite and silver-gold minerals, were deposited due to boiling of the fluid. The consequent decrease in temperature and increase in pH controlled deposition of quartz and calcite, respectively. Precipitation of silver and gold was caused by a combination of increased pH and oxygen fugacity, and a decrease in H_2S fugacity.

RÉSUMÉ

Le gîte d'Au-Ag de Shasta, situé dans la région de Toadoggone River dans le nord-centre de la Colombie Britannique, possède plusieurs caractéristiques des gisements épithermaux à basse sulfidation, de type adulaire-séricite. Le dépôt est constitué de réseaux de fissures remplies de quartz et calcite et de brèches, associés à des tufs dacitiques ayant subi une altération potassique. La minéralisation, principalement sous forme d'acanthite, d'électrum ainsi que d'argent natif, se retrouve dans des brèches de type Bonanza en association avec pyrite, sphalérite, chalcopryrite, galène, chlorite et hématite. Cependant, contrairement aux gîtes de type adulaire-séricite, le gisement de Shasta ne possède pas de veines d'adulaire et les plus fortes teneurs se retrouvent dans les brèches enrichies en calcite.

Les brèches hydrothermales, le quartz à grains fins et les inclusions fluides riches en vapeur sont de bonnes évidences pour l'ébullition des fluides circulant dans les veines. Les inclusions fluides indiquent une température de déposition des minéraux d'intérêt économique variant entre 280° et 225° C à une profondeur maximale de 750 m, à partir d'un fluide hydrothermal dilué. Une origine météorique du fluide est indiquée par les données isotopiques d'oxygène et d'hydrogène. Les conditions initiales estimées de $\log fO_2$ - pH montrent des valeurs comprises entre -33 et -31 et 4.25 et 6 respectivement, et auraient augmenté au cours du processus de minéralisation.

Le modèle de minéralisation proposé suggère que le quartz, suivi par la calcite et les minéraux aurifères et argentifères ont été déposés par conséquence de l'ébullition des fluides. Subséquentement, l'abaissement des températures et l'élévation du pH ont agi comme contrôles respectifs dans la deposition du quartz et de la calcite. La précipitation de l'argent et de l'or est le résultat d'une combinaison de facteurs incluant l'augmentation du pH et/ou de la fugacité de l'oxygène et/ou d'une diminution de la fugacité de H_2S .

ACKNOWLEDGEMENTS

First, I would like to thank my thesis advisor, A E Williams-Jones, for his energy and enthusiasm during this study. I would also like to thank several others at McGill for their time and effort on my behalf: Jim Clark of the Ixion Research Group Inc., for conducting various electron microprobe analyses and a thorough review of the original manuscript, Jim Mungall, for his assistance with the scanning electron microscope, Sandra Lalli and Constance Guignard, for geochemical assistance, Antoine Fournier, for French translation of the abstract; and George Panagiotidis, for rock sample preparation. I also want to acknowledge Steve Pezderic at the University of Saskatchewan, for performing stable isotope analyses, Acme Analytical Laboratories Ltd. of Vancouver, for geochemical whole-rock analyses, and Vancouver Petrographics Ltd. for thin section preparation.

Financial support was provided by Esso Minerals Canada Ltd. and Homestake Mining (Canada) Ltd. My sincere thanks are extended to John MacDonald, Robert Boyd, Ron Britten, Peter Holbek, Margaret McPherson and Henry Marsden for their interest and support. Additional funding was provided by NSERC and the B C Ministry of Energy, Mines and Petroleum Resources.

Last, but certainly not least, I would like to thank my parents, for their continuing encouragement and support.

PREFACE

This thesis consists of three chapters, the second of which is in manuscript form, and is intended for submission to a referred journal. My thesis advisor, A E Williams-Jones, is second author of the manuscript. His role in the preparation of the manuscript consisted of critical evaluation of the data and my interpretations presented therein, and editorial suggestions regarding organization of the text. I was employed by Esso Minerals and Homestake Mining at the Shasta deposit, and had access to geological maps and reports prepared by myself and other company geologists. This study, however, is based on detailed core logging and sampling, petrography and fluid inclusion analysis, conducted entirely by myself. Stable isotope analyses were conducted by Steve Pezderic at the University of Saskatchewan, and geochemical whole-rock analyses by Acme Analytical Laboratories of Vancouver. At McGill, Jim Clark provided sphalerite and chlorite compositional data from electron microprobe analyses, and Jim Mungal assisted with scanning electron microscope analyses.

TABLE OF CONTENTS

ABSTRACT	I
RÉSUMÉ	II
ACKNOWLEDGEMENTS	IV
PREFACE	V
TABLE OF CONTENTS	VI
LIST OF FIGURES	viii
LIST OF TABLES	xi
CHAPTER 1 INTRODUCTION	xii
General Statement	1
Objectives	3
Previous Work	4
Location and Access	4
Exploration History	5
CHAPTER 2 JOURNAL MANUSCRIPT	7
ABSTRACT	9
INTRODUCTION	10
GEOLOGICAL SETTING	11
Deposit Geology	15
Veins and Breccias	19
ALTERATION	22
Alteration Geochemistry	25
MINERALIZATION	28
Ore Mineralogy	29
Paragenesis	33
FLUID INCLUSIONS	33
Petrography	33
Origin	38
Microthermometry	39

Decrepitate Analyses	42
CHLORITE GEOTHERMOMETRY	43
STABLE ISOTOPES	46
Sulphur	46
Oxygen and Deuterium	48
DISCUSSION	51
P-T Conditions	51
Fluid Source	52
Source of Sulphur and Metals	55
fO_2 -pH Conditions	56
Fluid Evolution	59
Ore Transport and Deposition Controls	59
Deposit Model	63
Comparison with Other Low Sulphidation Deposits	65
SUMMARY AND CONCLUSIONS	67
CHAPTER 3 CONCLUSIONS	69
REFERENCES	72
APPENDIX I (Whole-rock Geochemical Data)	79
APPENDIX II (Fluid Inclusion Data)	81
APPENDIX III (Microprobe Analyses)	85

LIST OF FIGURES

Figure 1	Location map and geological setting of the Shasta deposit.	13
Figure 2	Simplified structure and stratigraphy of the Shasta deposit, modified after Marsden and Moore (1990).	17
Figure 3	An idealized cross section of the deposit, showing the approximate location of drill holes	18
Figure 4	Underground photographs of the hydrothermal breccias in the JM zone. The fragments are potassically altered wallrock, the dark grey matrix is high grade ore (quartz+calcite+chlorite), and the white matrix is later calcite. 4a) Note jigsaw textures and rotated angular fragments. 4b) Note the multiphase nature of the breccia and the crude banding around some fragments. Note hammer for scale.	20
Figure 5	Photographs of rock slabs showing textures of veins and breccias. 5a) Brecciated wall-rock healed by quartz-calcite, and later banded calcite and ore. 5b) Wall-rock fragment in high grade ore (consisting of sphalerite, chalcopyrite, acanthite and electrum), hosted by quartz-calcite±chlorite gangue, later calcite is banded and relatively low grade. Field of view is 15 cm.	21
Figure 6.	Photomicrographs of a potassically altered plagioclase phenocryst, replaced by K-feldspar, sericite and patchy calcite. Note relict albite twinning. 6a) Transmitted light, sericite is dark grey, K-feldspar medium grey, calcite white. 6b) Crossed polars, K-feldspar is dark grey, sericite grey, calcite white.	24
Figure 7.	A plot of TiO_2 vs Al_2O_3 in potassically altered rocks surrounding the JM zone. The excellent linear correlation shown by these oxides indicates that Ti and Al were essentially immobile during potassic alteration.	26
Figure 8	Gains and losses of K_2O , Na_2O , SiO_2 , and CaO , with assays of gold and silver, as a function of distance down diamond drill holes 89-09 and 89-10, which intersect the JM zone. Oxides have been normalized to constant Al, changes in mass were calculated relative to the least altered sample.	

	(89-09 #9, see App I) in the drill core The ore zone is shaded.	27
Figure 9	9a) A reflected light photomicrograph of euhedral pyrite grains hosted by early crystalline quartz and later calcite 9b) A transmitted light photomicrograph of ore minerals (sphalerite+galena+acanthite) precipitated at the contact between early quartz and later calcite in a narrow veinlet The wall-rock is at lower edge of the photograph Quartz, closest to vein wall, displays rounded grains (Sample CK84-14 70.3, see Fig 15)	30
Figure 10	Photomicrographs showing typical ore mineral textures 10a) Early euhedral pyrite, followed by sphalerite, chalcopyrite, and interstitial galena 10b) Sphalerite followed by chalcopyrite, and galena coprecipitated with acanthite (right side of photo). 10c) Early pyrite, which has been fractured and embayed and infilled by galena, acanthite and electrum 8d) Galena, acanthite, electrum and native silver precipitated after sphalerite Photographs a,b,c are in reflected light, d is an SEM TV image	31
Figure 11.	The paragenetic sequence of mineralization and alteration at Shasta	34
Figure 12.	Schematic representation of typical ore-breccia formation at Shasta.	35
Figure 13.	Photomicrographs of typical quartz-hosted inclusions (13a) and calcite-hosted inclusions (13b) Transmitted light	37
Figure 14.	Histograms of fluid inclusion microthermometric data and calculated fluid salinities for samples from mineralized zones (Oakes et al., 1990) T_h is the homogenization temperature, T_e is the eutectic or initial ice melting temperature, $T_{m, ice}$ is the final ice melting temperature	40
Figure 15.	The distribution of T_h for L-V inclusions across two narrow veinlets in the Creek zone The dotted line represents mineralization in sample CK84-14 70 3, (see Fig 9b)	41
Figure 16.	Microphotograph of a typical fluid inclusion decrepitate observed in this study Bladed crystals are KCl, groundmass is NaCl and $CaCl_2$	45

Figure 17	A plot of δD vs $\delta^{18}O$ showing the estimated composition of the Shasta fluid and water/rock ratio. The latter was calculated assuming the fluid was of meteoric origin and was isotopically modified as a result of interaction with surrounding volcanic wall rocks	54
Figure 18	Log fO_2 - pH diagram constructed at 280°C, showing the predominance fields for aqueous sulphur species, and stability fields for minerals in the Fe-S-O system, K-feldspar, muscovite and calcite. $\Sigma[S]= 0.01m$, $[K]= 0.1 m$, and $I= 0.5$ based on decrepitate and microthermometric data. $\Sigma[C]= 0.001 m$, is an assumed value (see text for more detail). Thermodynamic calculations were performed using the computer program SUPCRIT92 (Johnson et al, 1992). Contours of $\delta^{34}S_{H_2S}$ were calculated using the data of Ohmoto (1972) and an assumption that $\Sigma\delta^{34}S=0$. The horizontal "2‰ FeS" line in the pyrite field reflects the iron content in sphalerite. The shaded area represents the probable initial fluid conditions, discussed in the text. The thick contour line represents the range in pH and log fO_2 conditions constrained by $\delta^{34}S_{H_2S}$ values.	58
Figure 19	Log fO_2 - pH diagrams constructed at 280°C and 225°C, under the same conditions as Fig. 18, showing gold solubility contours calculated using the data of Seward (1973).	60
Figure 20.	Log fO_2 - pH diagrams constructed at 280°C and 225°C, under the same conditions as in Fig. 18, showing the boundary between acanthite and native silver, and silver solubility contours calculated using the data of (Gammons and Barnes 1989)	61
Figure 21	Conceptual model of the Shasta deposit.	64

LIST OF TABLES

Table 1.	Fluid Inclusion Decrepitate Data	44
Table 2.	Sulphur Isotope Data	47
Table 3.	Oxygen and Hydrogen Isotope Data	49

CHAPTER 1 INTRODUCTION

General Statement

Although Lindgren first proposed the term "epithermal" in 1933 to describe a class of precious and base metal mineral deposits, only in the last decade have we begun to fully understand the genesis of these valuable ore deposits. The various morphologies of epithermal deposits have been described by Buchanan (1981) and Berger and Eimon (1983), and the relationship between these deposits and active geothermal systems has been established by authors such as White (1974, 1981), Henley (1985), Henley and Ellis (1983), Hedenquist (1987), and Clark and Williams-Jones (1990). Two general classes of epithermal deposits are now recognized, termed acid-sulphate and adularia-sericite (Hayba et al., 1985) based on mineralogy and alteration styles; or alternatively termed high or low sulphidation (Hedenquist, 1987) based on interpreted fluid chemistry.

The study of active geothermal systems has contributed significantly to the development of comprehensive models for the "fossil" hydrothermal systems which constitute many epithermal deposits. It is now generally accepted that most epithermal deposits are formed by predominantly meteoric waters (White, 1974), carrying precious and base metals in solution mainly as bisulphide and chloride complexes, respectively (Seward, 1989), and that mineral deposition can be controlled by fluid mixing, wall rock interaction or boiling of the hydrothermal fluid (Drummond and Ohmoto, 1985, Reed and Spycher, 1985). Mixing of

hydrothermal fluids with ground water generally causes cooling and dilution of the mineralizing fluid, which is interpreted to have been responsible for precious and base metal deposition at Round Mountain, Nevada (Sander and Einaudi, 1990) and at Creede, Colorado (Hayba et al , 1985) Wall rock interaction can affect solution pH and/or redox state, the latter of which has been invoked as a control on gold deposition in some banded iron-formations (Phillips and Groves, 1984). Boiling of the hydrothermal fluid also affects solution pH and redox state, as well as temperature and salinity, and has been cited as the critical control on gold-silver and base metal mineralization in epithermal deposits such as the Finlandia Vein, Peru (Kamilli and Ohmoto, 1977), Golden Cross, New Zealand (de Ronde and Blattner, 1988) and Guanajuato, Mexico (Buchanan, 1979)

Shasta is an economic Ag-Au deposit similar in many respects to the adularia-sericite type deposits described by Hayba et al (1985) and Heald et al (1987) The ore minerals consist of acanthite, electrum and native silver, accompanied by chlorite and minor base metal sulphides These are hosted by quartz-calcite stockwork and hydrothermal breccia veins, associated with potassic and sericitic wall rock alteration

However, certain features of the Shasta deposit differ from those of typical epithermal mineralization. For example, mercury, arsenic and antimony are not enriched in the deposit, nor are sulphosalt minerals present The deposit contains abundant calcite, but it lacks vein adularia and lamellar quartz (replacing calcite). Moreover, calcite-rich breccias host some of the highest ore

grades at Shasta, a feature that is not common in the majority of epithermal deposits described in the literature (Silberman and Berger, 1985; Hayba et al., 1985)

Silver and gold mineralization is concentrated in Bonanza-type hydrothermal breccias at Shasta, which suggests that boiling played a significant role in mineral deposition. Boiling is often cited as a control on mineralization in epithermal deposit studies, but the specific factors associated with boiling that directly affect mineral deposition, such as temperature, pH, oxidation state, etc., are rarely evaluated systematically. The Shasta deposit therefore provides an opportunity to investigate an unusual style of epithermal mineralization not previously described, and to document the specific controls on silver-gold deposition in a boiling hydrothermal system.

Objectives

This thesis was undertaken to investigate the genesis of the Shasta deposit, in order to contribute to a refined model for epithermal deposits in the Toadoggonne River area and similar settings, and to document the specific controls on mineralization in an unusual type of epithermal deposit.

The objectives of this study were to determine the paragenesis of mineralization and wall-rock alteration; characterize the hydrothermal fluids and environment of deposition, identify the specific controls of mineralization; and propose a genetic model for the deposit. This has been accomplished through

a combination of surface and underground mapping and sampling, drill core logging and sampling, whole rock geochemistry, petrography, fluid inclusion microthermometry, fluid inclusion decrepitate analyses, stable isotope analyses for sulphur, oxygen and hydrogen, and thermodynamic analysis of phase relationships

Previous Work

The regional geology and metallogeny of the Toodoggone district has been described by Carter (1972), Gabrielse et al (1976), Panteleyev (1982, 1983), Schroeter (1982), Diakow (1984), Diakow (1984, 1990), Diakow et al (1985; 1991), Forster (1984) and Clark and Williams-Jones (1987, 1988) The stratigraphy and structure of the Shasta deposit has been documented by Marsden and Moore (1989, 1990) and Marsden (1990) Previous workers have also described several other epithermal deposits in the Toodoggone district (Barr, 1978, Baker mine, Forster, 1984, Moosehorn and Mt Graves prospects, Clark and Williams-Jones, 1986, Bonanza deposit, Vulimuri et al , 1987, Lawyers mine) but none of these studies have provided detailed evaluation of the immediate controls on mineralization.

Location and Access

The Shasta deposit is located in the Toodoggone River area of northern British Columbia (Fig. 1), on NTS map sheets 94E\2,3,6,7, centred at latitude

57'15' north, longitude 127'00' west. The property is accessible by gravel road from the Sturdee Airstrip, 9 km to the south, (approximately 300 km by air, north of Smithers, BC), or via the Omineca mine road controlled by Cheni Gold Mines Ltd., some 675 km north-west of Ft. St. James. The property straddles Jock Creek valley which has moderately steep slopes, and lies between elevations 1250 m and 1750 m. The area was swept by forest fire some 30 years ago, and is now vegetated by low brush and alpine grass.

Exploration History

The Toadoggone district was the focus of major exploration activity during the 1980's, and became an important silver-gold mining camp during that time. Between 1980 and 1983, Dupont Canada Inc. produced 37,558 oz gold and 742,210 oz silver from 77,500 tons of ore in quartz veins at the Baker (Chappelle) mine (Schroeter et al., 1986), and Cheni Gold Mines Ltd. operated until 1992 based on ore reserves of 1.9 million tons of 0.198 oz/ton gold and 7.09 oz/ton silver (Shareholders Report 1989) from quartz stockwork-breccia veins at their Lawyers mine.

The Shasta property was initially staked in 1972, and is currently owned by International Shasta Resources Ltd. The deposit has been explored by Newmont Exploration of Canada (1983), Esso Minerals Canada (1987-1989), and most recently by Homestake Canada (1990-1991). Reserves at Shasta have been estimated by McPherson et al. (1991) at 1.6 million tonnes of ore.

containing 2.84 grams per tonne gold and 132.2 grams per tonne silver. International Shasta Resources conducted mining operations on the deposit during 1989 and 1990, removing approximately 78,500 tonnes of high grade ore.

CHAPTER 2: JOURNAL MANUSCRIPT

**Mineralization and Ore Controls
of the Shasta Ag-Au Deposit,
Toodoggone River Area, British Columbia**

by

Peter C. Thiersch and A.E. Williams-Jones

**Department of Earth and Planetary Sciences
McGill University
Montreal, Quebec
Canada
H3A 2A7**

ABSTRACT

The Shasta epithermal Ag-Au deposit, located in the Toodoggone River mining district of British Columbia, consists of quartz-calcite stockwork-breccia zones, associated with K-silicate wall-rock alteration, and hosted by dacitic lapilli tuffs and flows. The deposit has many characteristics of low-sulphidation adularia-sericite type deposits, but the lack of vein adularia and the strong association between ore grades and calcite-rich hydrothermal breccias is atypical.

Ore stage mineralization consists of pyrite, sphalerite, chalcopyrite, galena, acanthite, electrum, native silver and chlorite, in mixed quartz-calcite veins and hydrothermal breccias. Pre-ore and post-ore veins consist only of quartz, and calcite, respectively. Microthermometric analyses of fluid inclusions indicate that ore stage mineralization was deposited between 280°C and 225°C from a relatively dilute hydrothermal fluid (1-5 wt% NaCl eq.). Abundant vapour-rich inclusions in ore stage calcite suggest that boiling played a significant role in ore deposition. $\delta^{18}\text{O}_{\text{fluid}}$ (-1.5 to -4.1‰) and $\delta\text{D}_{\text{fluid}}$ (-148 to -171‰) values indicate that the fluid had a meteoric origin, but was strongly enriched in ^{18}O due to extensive wall-rock interaction. $\delta^{34}\text{S}$ values for pyrite associated with ore mineralization show a significant trend to lower values with increasing ore grade, which is interpreted as evidence for increasing $f\text{O}_2$ conditions during ore deposition. Initial conditions of the mineralizing fluid were estimated to lie between pH 4.25 to 6.0 and $\log f\text{O}_2$ -33 to -31 at 280°C, during ore deposition, the fluid evolved to more alkaline and oxidizing conditions.

A model is proposed in which hydrothermal fluids were localized by extensional faults, and ore deposition was controlled by decompressional boiling in response to throttling and/or hydro-brecciation. Calcite was precipitated in abundance because of the increase in pH that accompanied boiling. Base metal sulphides were also deposited as a result of the increase in pH, the associated increase in oxidation state, and decrease in H_2S concentration lead to precipitation of gold and silver.

INTRODUCTION

Epithermal gold-silver deposits have recently been divided into two broad classes, termed acid-sulphate and adularia-sericite by Hayba et al (1985) and Heald et al (1987), based on mineralogy and alteration styles, or alternatively termed high sulphidation and low sulphidation by Hedenquist (1987), based on interpreted fluid chemistry. According to these classification schemes, acid-sulphate or high sulphidation deposits are characterized by the presence of enargite+pyrite, abundant hypogene alunite and an advanced argillic alteration assemblage, whereas adularia-sericite or low sulphidation deposits are distinguished by the lack of hypogene alunite and presence of acanthite, adularia and chlorite, and a sericitic alteration assemblage. In this paper, we describe an epithermal deposit which has some affinity to the low sulphidation adularia-sericite class, but differs from typical deposits in several important respects.

The Shasta silver-gold deposit consists of acanthite, electrum, native silver, chlorite and minor base metal minerals, hosted by quartz-calcite stockwork and breccia veins. Wall-rocks have been altered to K-silicate assemblages (K-feldspar+sericite). However, the deposit lacks vein adularia, a common component of the low sulphidation class, and the highest grades of silver and gold mineralization are associated with a transition from quartz to calcite deposition in veins and breccias, which is also atypical (Silberman and Berger, 1985, Hayba et al., 1985, Heald et al., 1987).

The model most commonly proposed to explain the the genesis of

adularia-sericite type deposits involves boiling of the hydrothermal fluid, leading to deposition of silver-gold mineralization in chalcedonic quartz veins containing adularia (Buchanan, 1981) It appears that boiling was also the dominant cause of Ag-Au deposition at Shasta, since high grade mineralization is associated with intense hydrothermal brecciation. However, in contrast to most adularia-sericite type deposits, deposition of quartz was largely complete before the hydrothermal fluid became saturated with respect to ore minerals.

This paper makes use of various types of geochemical information (including mineral and whole-rock chemical analyses, fluid inclusion microthermometry, and stable isotope analyses) to develop a model in which progressive boiling of a low salinity, relatively acidic fluid produced a sharp initial drop in temperature followed by more gradual increases in pH and oxygen fugacity. According to this model, quartz was deposited immediately as a result of the drop in temperature, whereas deposition of calcite and the ore minerals occurred later, due to evolution of the fluid to higher pH and fO_2

GEOLOGICAL SETTING

The Shasta deposit is located in the Toodoggone River district of north-central British Columbia within the Stikine Terrane, which consists of Late Paleozoic to Mesozoic island-arc volcanics and overlying sedimentary rocks (Fig. 1) In the Toodoggone area, Late Triassic Stuhini Group and Early to Middle Jurassic Hazelton Group volcanics and coeval Omineca intrusions are overlapped

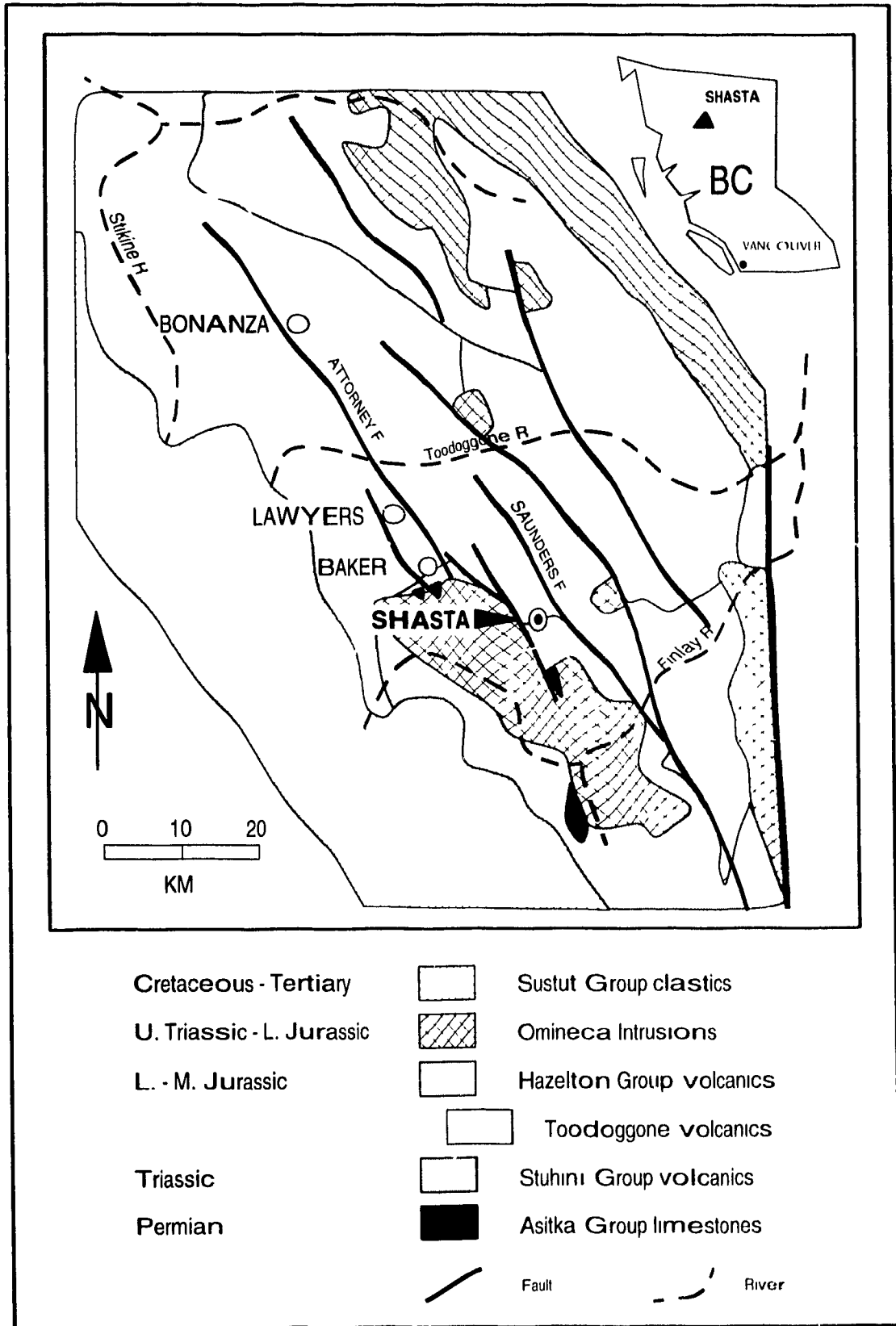
to the south-west by Middle to Upper Jurassic Bowser and Upper Cretaceous Sustut successor basins (Tipper and Richards, 1976, Gabrielse et al , 1976) Most of the significant precious metal deposits in the area, including Shasta, are hosted by the Toodoggone volcanics (Carter, 1972) which represent a distinctive quartz-bearing facies of the Hazelton Group

The regional structure and stratigraphy of the Toodoggone district has been described in detail by Carter (1972), Gabrielse et al (1976), Panteleyev (1982, 1983), Schroeter (1981, 1982), Diakow (1984, 1990), and Diakow et al. (1985; 1991); only a brief summary is provided here

The oldest rocks in the immediate study area are Early (?) Permian limestones of the Asitka Group, which generally occur in thrust contact with Late Triassic Stuhini Group volcanics and as roof pendants within Omineca intrusions Stuhini Group rocks are dominantly submarine porphyritic augite basalt flows, with intercalated tuffs and volcanic breccia. Unconformably overlying the Stuhini are Early to Middle Jurassic Hazelton Group rocks, comprising mainly subareal andesitic to dacitic flows, tuffs, lahars and epiclastic rocks.

The Toodoggone volcanics form a northwest-trending belt 2 to 20 km wide and 90 km long, and are estimated to be more than 2200 metres thick (Diakow, 1990). They comprise generally subaerial, andesitic to dacitic ash-flow tuffs and lava flows, with intercalated volcanic sandstones, conglomerates and lahars. These rocks have been subdivided into the Moyez, Metsantan, McClair, Attycelley and Saunders members, based on stratigraphic evidence and

Figure 1. Location map and geological setting of the Shasta deposit.



published K-Ar ages (Diakow, 1990).

Early Jurassic Omineca intrusions, such as the Black Lake stock, situated 2 km west of the deposit, comprise granodiorite, quartz monzonite and quartz diorite stocks and plugs which intrude Asitka and Stuhini Group rocks. The youngest rocks in the area are chert pebble conglomerates of the Middle to Upper Cretaceous Sustut Group, which unconformably overlie the Toodogone volcanics.

Recent research by Clark and Williams-Jones (1990) has constrained the age of the Toodogone volcanics to a narrow interval between 198 and 193 Ma using ^{40}Ar - ^{39}Ar dating methods. Their data also indicates that acid-sulphate type mineralization, such as that in the Bonanza deposit (196 Ma), was contemporaneous with volcanism, but that Shasta (187 Ma) and adularia-sericite type deposits such as Lawyers (188-190 Ma), formed up to several million years after the cessation of the main stage of volcanism.

The Toodogone volcanics are relatively undeformed and unmetamorphosed. Strata dip shallowly (~25 degrees) to the north-west. The dominant structures are north to north-west trending, steeply dipping dextral strike-slip faults, concordant with the primary tectonic fabric of the Stikine Terrane. One of these structures, the Saunders fault, borders the Shasta deposit to the east, and shows up to 5 km of right lateral displacement (Diakow et al., 1985).

Several of the Toodogone area deposits, including Lawyers, Baker and

Shasta, lie near northwest trending faults (Fig 1) Diakow (1990) proposed that these deposits lie along the margin of the "Central Toadogone Depression" a fault-bounded trough which may have ponded later volcanics and localized hydrothermal fluids during extension. In the case of the Lawyers deposit, Vulimuri et al. (1985) cited structural and stratigraphic evidence for graben formation, proposing that northwest trending block faults were probable structural controls for mineralization. At Shasta, structurally controlled zones of mineralization share a similar northwest trend, which supports the hypothesis that this style of faulting may have played a significant role in localizing mineralization at both regional and deposit scales in the Toadogone district

Deposit Geology

The Creek and JM zones are the largest of a dozen mineralized zones that comprise the Shasta deposit (Fig. 2) They also constitute the bulk of mineralization, containing an estimated 1.6 million tonnes with an average grade of 2.84 g/t Au and 132.2 g/t Ag (McPherson et al , 1991)

The zones are generally tabular in shape, and are more continuous laterally than vertically. The Creek zone strikes 180° with a length of 875 m, dipping 60° west and continuing 300 m down-dip. The JM zone strikes 330° over a distance of 1000 m, dipping 70° east to 70 m depth. These attitudes produce an inverted "V" geometry which plunges shallowly to the northwest (Fig 3)

The deposit is hosted by rocks that are probably equivalent to the

Attycelley unit, described by Diakow (1990) as green to mauve lapilli-ash tuffs and lapilli-block tuffs with minor ash-flows, lava flows and epiclastic rocks. Marsden and Moore (1990) investigated the stratigraphy and structure in detail; only a brief summary is provided here

The strata can be divided into four units which unconformably overly rocks of the Stuhini Group (Fig. 2) They are, from oldest to youngest. 1) a homogenous feldspar-quartz-biotite porphyry; 2) heterogeneous feldspar-quartz lapilli tuffs, 3) lahars, crystal tuffs and epiclastic rocks; and 4) welded lapilli tuff. All mineralization is restricted to the first two units.

The lowermost feldspar-quartz-biotite porphyry and overlying feldspar-quartz lapilli tuffs are about 300 m thick. They are dacitic in composition, and contain characteristically salmon-pink coloured plagioclase feldspar in a pale green matrix with variable lapilli content. Marsden and Moore (1990) proposed that this package represents a dacite dome complex, consisting of an extrusive porphyry dome overlapped by coeval pyroclastic rocks. The laharic unit is roughly 200 m thick, and overlies the pyroclastic rocks in apparent unconformity. It consists of hematite-rich heterolithic lahars, intercalated feldspar crystal tuffs and fine grained volcanic sediments. The uppermost unit is a chloritic, variably welded feldspar crystal lapilli tuff. The rapid lateral and vertical facies changes observed in these lithologies are typical of stratovolcanoes, where dacitic to andesitic flows and pyroclastics are commonly interbedded with reworked volcanic sediments (Cas and Wright, 1988).

Figure 2. Simplified structure and stratigraphy of the Shasta deposit, modified after Marsden and Moore (1990).

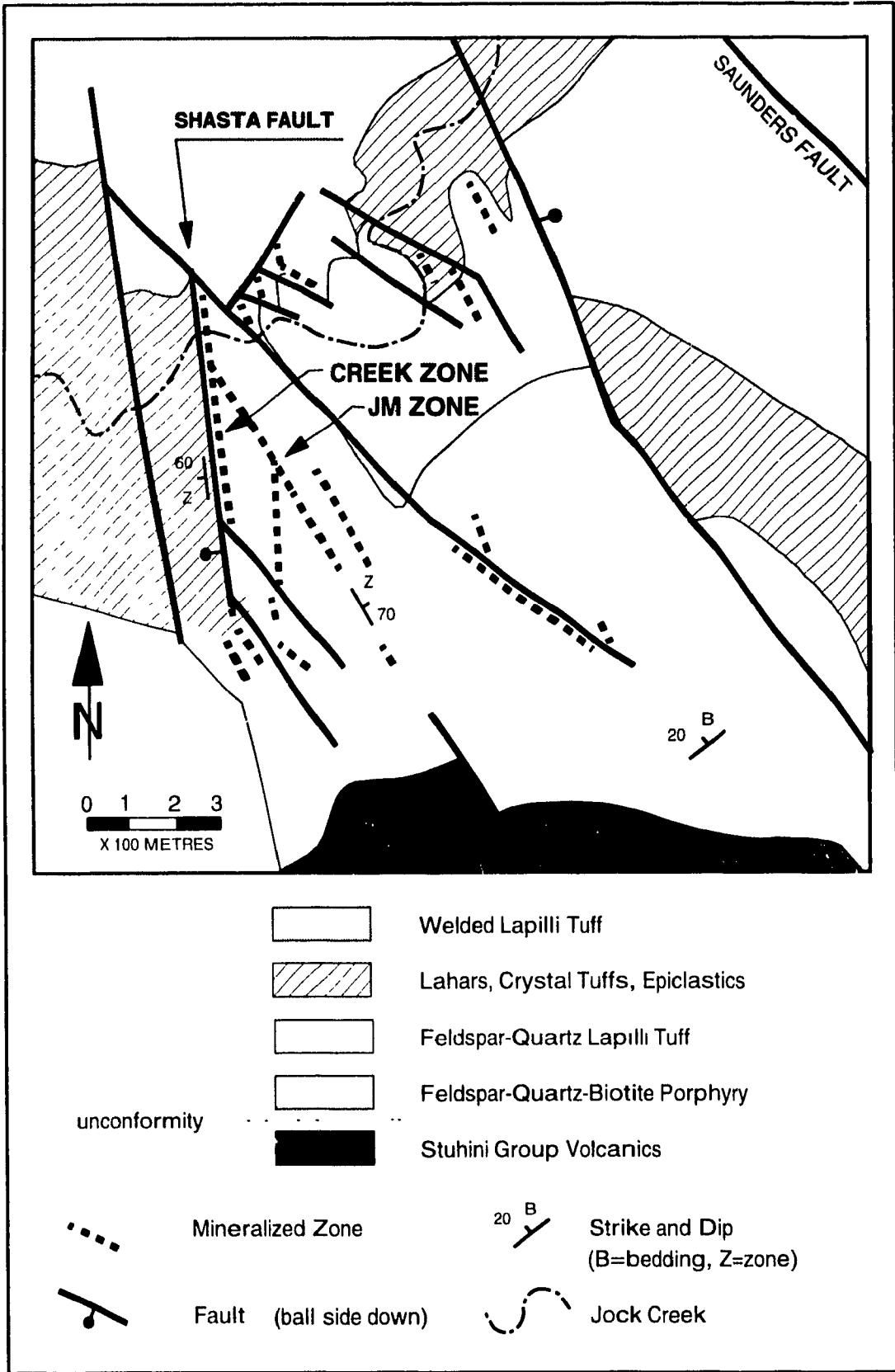
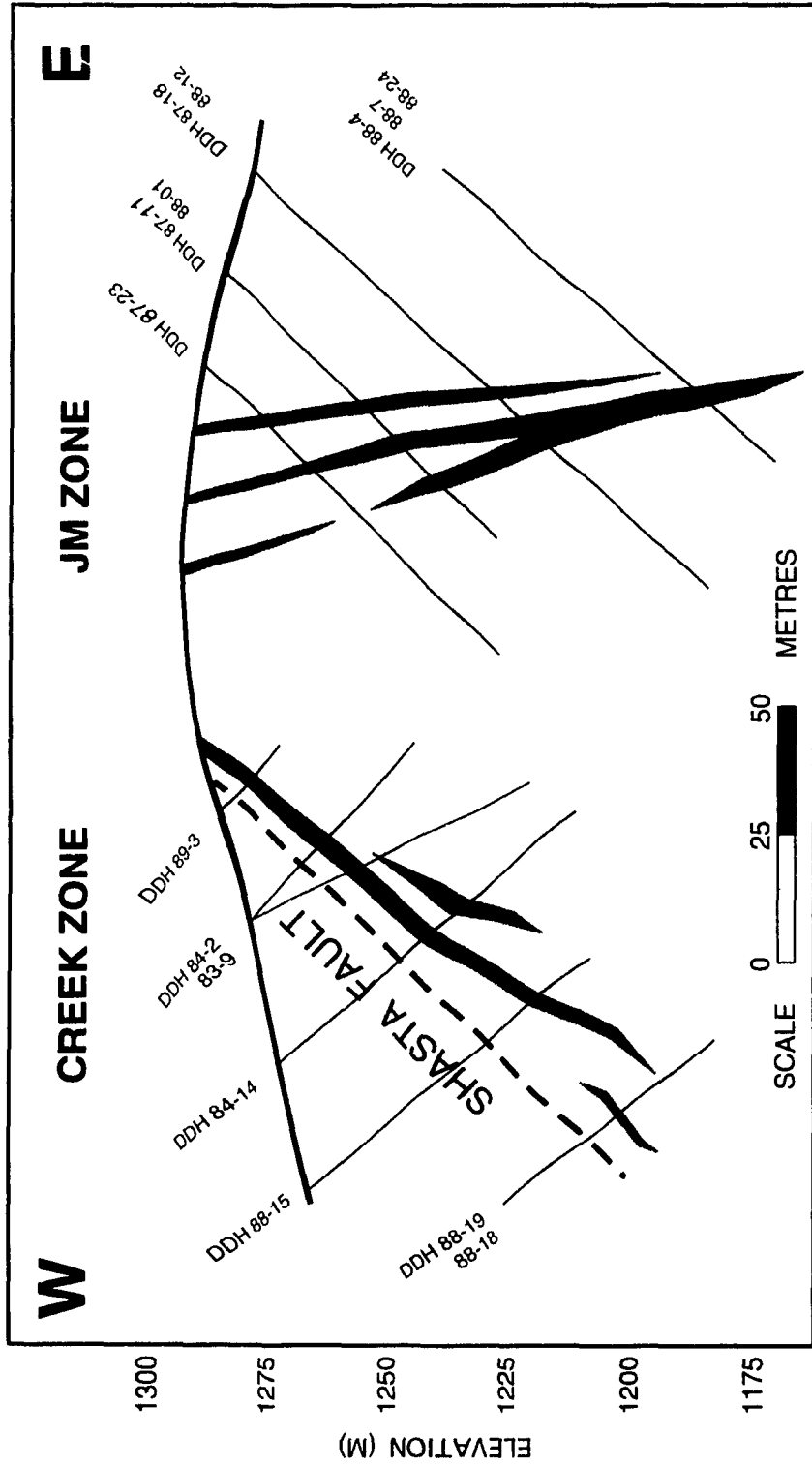


Figure 3. An idealized cross section of the deposit, showing the approximate location of drill holes.



The structure of the deposit area is dominated by north to northwest trending normal and/or dextral strike-slip faults. All mineralized zones are hosted by structures that are sub-parallel to these faults, later northeast trending faults truncate mineralization. Strata surrounding the deposit generally dip shallowly to the northwest, concordant with the regional attitude.

The most obvious structure is the Shasta fault, which strikes 180° and dips 50° to the west, separating pyroclastic host rocks in the footwall from overlying epiclastic rocks in the hangingwall (Fig 2). The Shasta fault displays post-mineralization movement, forming the hangingwall to the Creek zone near surface, but curves away from this zone at depth. In the JM zone, a late carbonate vein (the CB vein) forms the hangingwall to ore mineralization. The vein is essentially parallel to the zone and is semi-continuous over 200 metres, varying from a 1.5 metre wide vein to a 15cm wide gouge filled seam.

Given that both the CB vein and the Shasta fault are parallel to zones of mineralization and form the hangingwall in both cases (Fig 3), it is likely that these fissures were the result of recent movement on structures that initially produced zones of fracture-controlled permeability that focussed the hydrothermal fluids.

Veins and Breccias

Mineralized zones consist of crosscutting, multi-stage quartz-calcite stockwork and breccia veins. Stockwork zones, up to 30 m wide, are enclosed

Figure 4 Underground photographs of the hydrothermal breccias in the JM zone. The fragments are potassically altered wallrock, the dark grey matrix is high grade ore (quartz+calcite+chlorite), and the white matrix is later calcite. 4a) Note jigsaw textures and rotated angular fragments. 4b) Note the multiphase nature of the breccia and the crude banding around some fragments. Note hammer for scale.

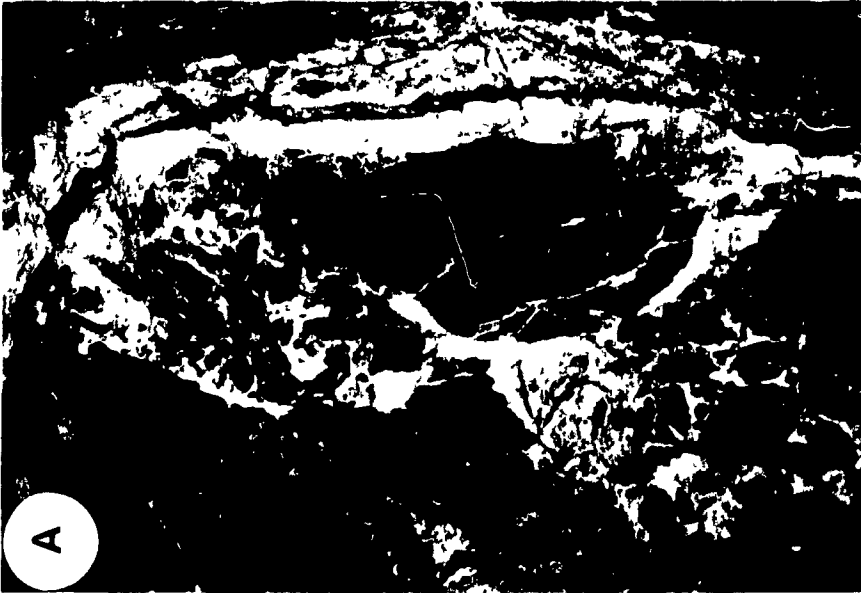
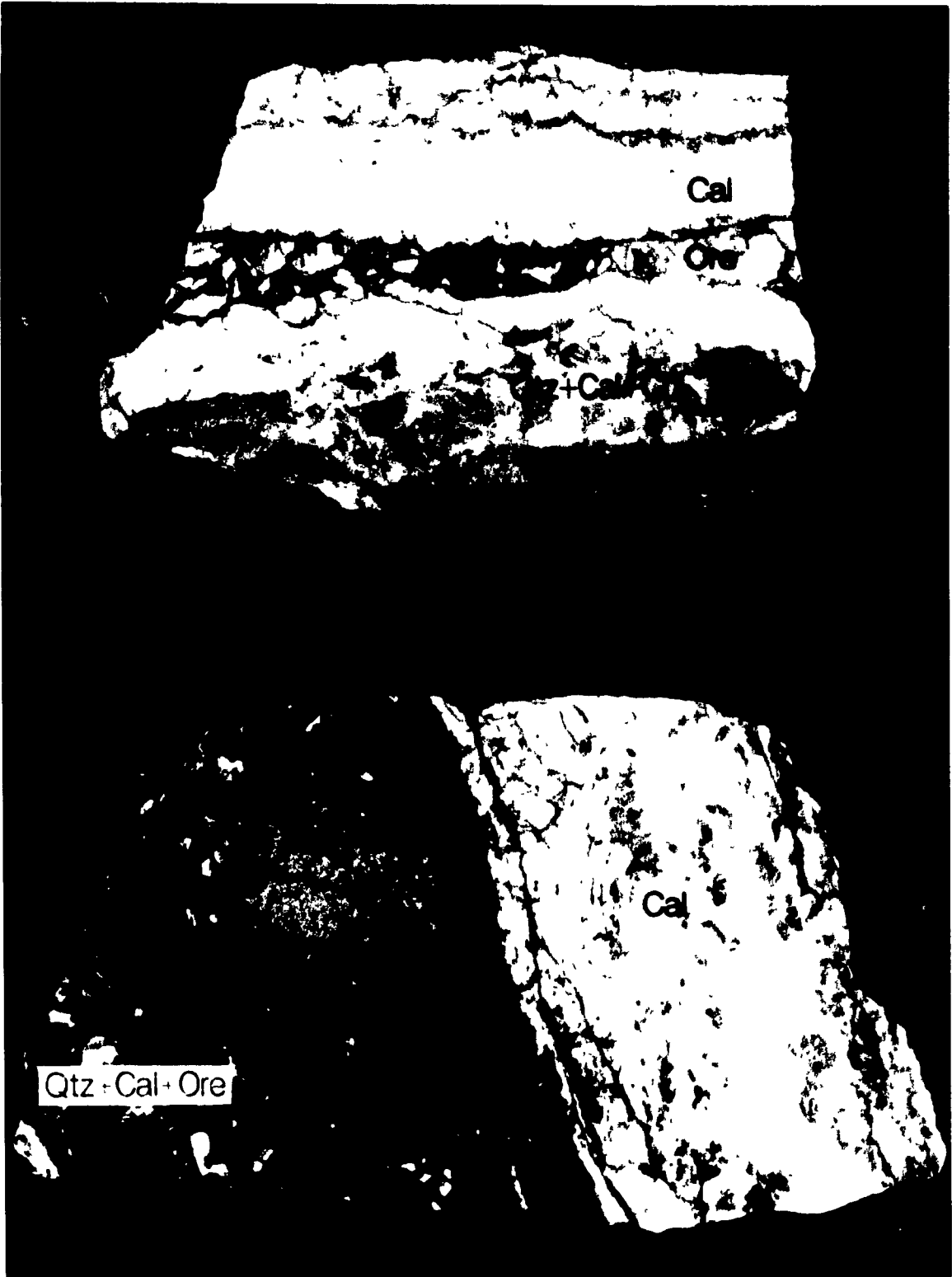


Figure 5. Photographs of rock slabs showing textures of veins and breccias. 5a) Brecciated wall-rock healed by quartz-calcite, and later banded calcite and ore. 5b) Wall-rock fragment in high grade ore (consisting of sphalerite, chalcopryite, acanthite and electrum), hosted by quartz-calcite±chlorite gangue; later calcite is relatively low grade. Field of view is 15 cm.



by generally tabular, salmon-pink coloured alteration zones up to 100 m wide. Stockwork veins are massive to crudely banded and 1 to 75 centimetres wide. Breccia veins pinch and swell along strike and down dip within the stockwork zones, forming discontinuous, subparallel or en echelon pods up to 15 metres wide. They typically grade outward into stockworks (defined as containing less than 50% vein material) but also crosscut earlier stockwork veins. The breccias consist of hydrothermally altered wall-rock and vein material fragments in a matrix of vein gangue. They range from narrow, single-stage breccias of "jigsaw" type, to wider, multi-stage breccias of repeatedly fractured and re-cemented fragments 1 to 100 centimetres in size (Fig. 4, 5). The matrix generally lacks clay gouge or rock flour.

ALTERATION

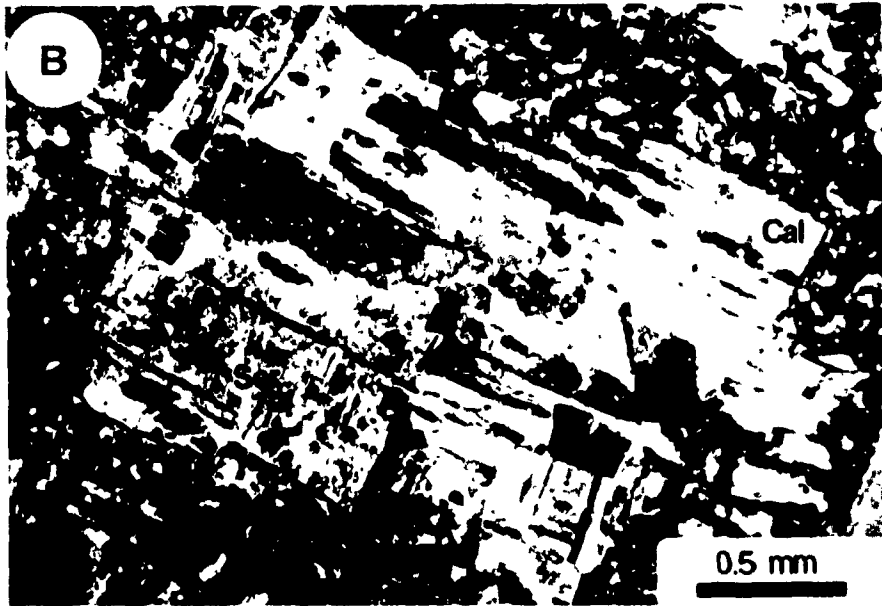
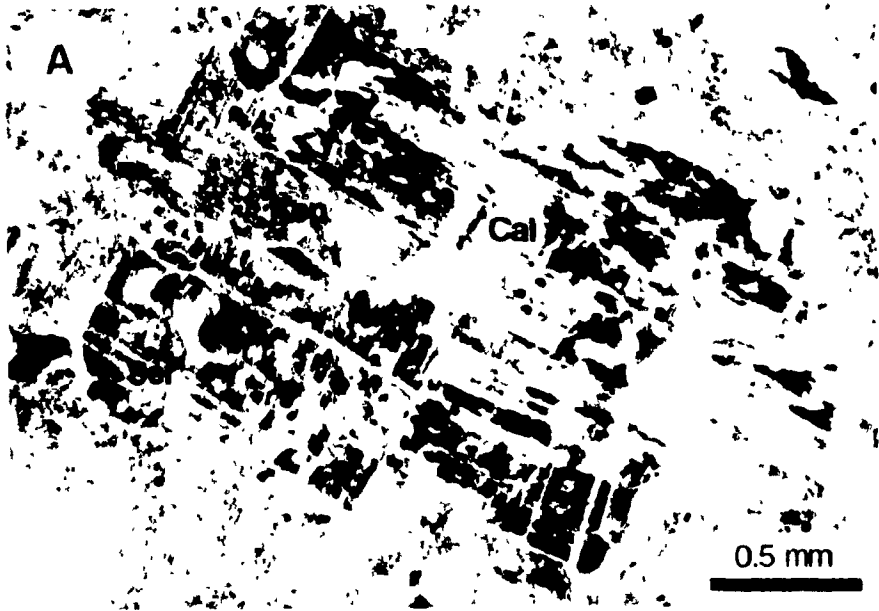
Hydrothermal alteration associated with the deposit can be classified as propylitic, potassic, and sericitic, based on the mineral assemblages described below. Propylitic alteration is regional in extent, and grades into potassic alteration over several metres, proximal to the deposit. Potassic alteration is directly associated with quartz stockwork veins and forms broad salmon-pink haloes that surround stockwork zones. Sericitic alteration locally overprints potassically altered zones but is irregularly distributed and not well documented. The typical epithermal trace elements mercury, arsenic and antimony (Silberman and Berger, 1985) are not significantly enriched within the alteration haloes.

Propylitic alteration consists of an assemblage of chlorite, epidote, calcite and pyrite, which imparts a pale green colour to the affected rock. Typically, lapilli are strongly chloritized and plagioclase phenocrysts are replaced by fine-grained chlorite and epidote, but primary textures are preserved.

Potassic alteration is characterized by replacement of plagioclase phenocrysts and lapilli by K-feldspar, sericite and minor calcite (Fig 6) and pervasive silicification of the groundmass. Propylitically chloritized lapilli and biotite phenocrysts are typically replaced by sericite and pyrite. The intensity of alteration is directly dependent on quartz vein density and, in areas of high vein density, secondary K-feldspar and quartz completely obscure primary textures and impart a deep red colour to the affected rock. Primary textures are preserved only in weakly to moderately altered zones. Epidote is an accessory mineral in weakly altered zones, where it occurs as fine veinlets and disseminations. Pale green illite is commonly observed on late fractures and fills rare vugs in potassically altered zones.

Sericitic alteration was observed as narrow haloes (<2 m) surrounding late, high grade calcite breccias in the JM zone, but also as irregular patches apparently unrelated to mineralization. The sericitic assemblage consists of fine-grained sericite, quartz and pyrite which have completely replaced the original mineralogy and generally destroyed primary textures. This alteration style has produced soft, tan coloured zones with relatively sharp boundaries.

Figure 6 Photomicrographs of a potassically altered plagioclase phenocryst, replaced by K-feldspar, sericite and patchy calcite. Note relict albite twinning. 6a) Transmitted light, sericite is dark grey, K-feldspar medium grey, calcite white. 6b) Crossed polars, K-feldspar is dark grey, sericite grey, calcite white.



Alteration Geochemistry

Bulk whole-rock geochemical analyses were conducted on samples of core taken from two drill intercepts of the JM zone (ddh 89-09 and 89-10), to determine the distribution of selected elements across the potassic alteration halo that surrounds mineralized stockwork-breccia zones. The samples consisted of assay pulps, which represent continuous, 1-2m long intervals of core through the hangingwall, ore zone and footwall of the JM zone. Analyses were conducted at Acme Laboratories in Vancouver, B.C., using Induced Coupled Plasma (ICP) techniques for whole rock oxides and fire assay (with atomic absorption finish) for gold and silver, these data are presented in Appendix I.

The linear correlation between TiO_2 and Al_2O_3 (Fig 7) suggests that aluminum was relatively immobile during potassic alteration. Thus, for the purpose of comparison and to correct for the effects of any changes in volume, results for the other oxides were normalized to constant aluminum. Their masses were balanced relative to the least altered sample (89-10 #9) in order to determine the net changes in bulk rock composition during potassic alteration. The corrected data show that up to 240 wt% of SiO_2 and 170 wt% CaO were added in the ore zone intersected by ddh 89-10, reflecting the high density of quartz and calcite veins in the stockwork zone (Fig. 8) High Ag-Au contents are not everywhere related to quartz vein density, however, as seen in the minor addition of silica in the ore zone intersected in ddh 89-10 In this hole, there is nevertheless a sharp increase in CaO across the ore zone, however, which

Figure 7 A plot of TiO_2 vs Al_2O_3 in potassically altered rocks surrounding the JM zone. The excellent linear correlation shown by these oxides indicates that Ti and Al were essentially immobile during potassic alteration

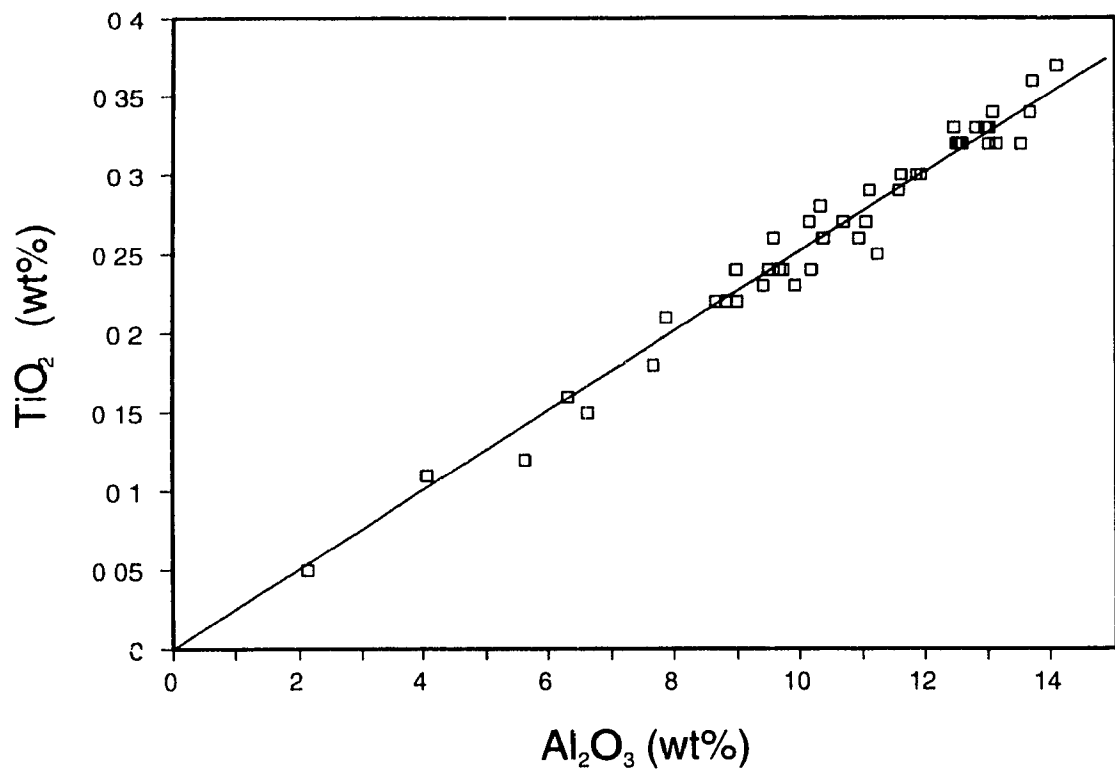
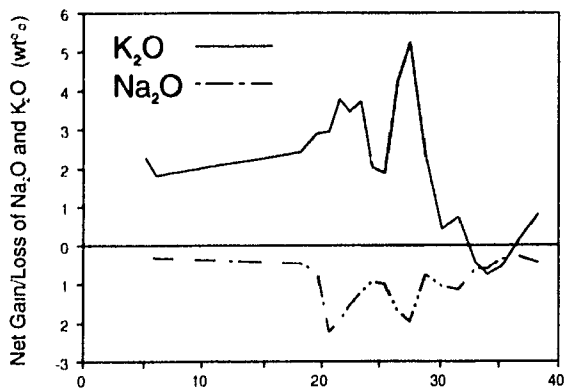
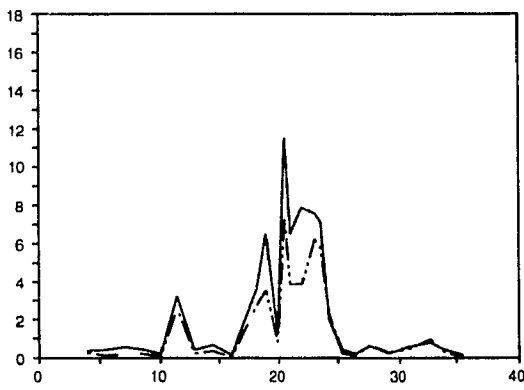
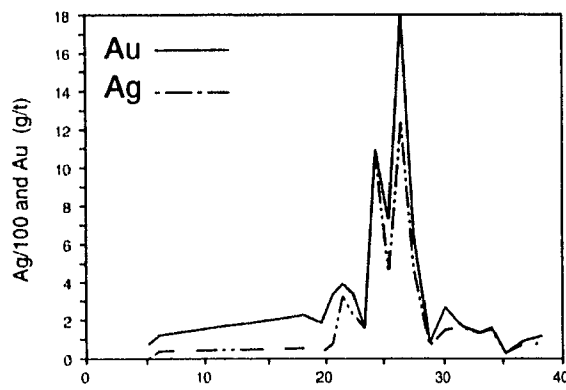
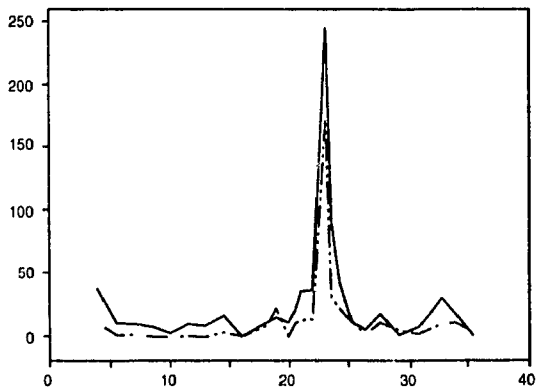
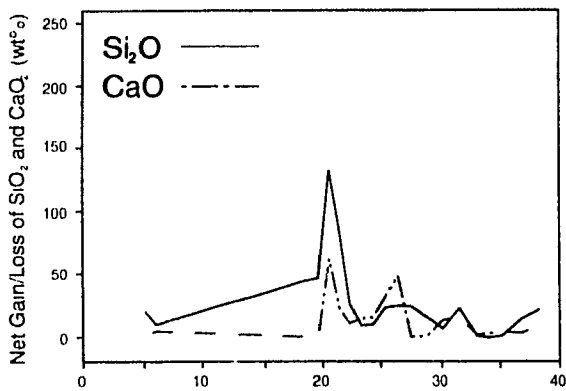
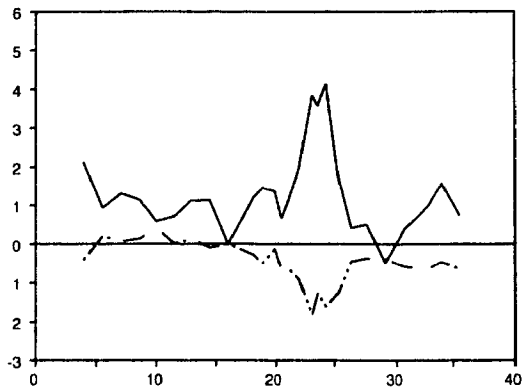


Figure 8. Gains and losses of K_2O , Na_2O , SiO_2 , and CaO , with assays of gold and silver, as a function of distance down diamond drill holes 89-09 and 89-10, which intersect the JM zone. Oxides have been normalized to constant Al, changes in mass were calculated relative to the least altered sample (89-09 #9, see App I) in the drill core. The ore zone is shaded.

DDH 89-09



DDH 89-10



Depth Down Hole (m)

Depth Down Hole (m)

reflects the strong association of calcite with ore mineralization. Histograms of K_2O and Na_2O show that up to 5 wt% K_2O was added and 2 wt% Na_2O lost in the ore zones, which is consistent with the observed replacement of plagioclase by K-feldspar and sericite in potassically altered zones.

MINERALIZATION

Gangue minerals in veins and breccias consist of quartz and calcite in roughly equal proportions, but a spatial zonation of these minerals is apparent from drill intercepts. Quartz is dominant at higher elevations and in the periphery of stockwork zones, whereas calcite is more abundant at lower levels and in central breccias. Quartz is characteristically fine grained and locally chalcedonic, whereas calcite tends to be relatively coarse grained. Both minerals display open space-filling textures of well formed crystals and cock's combs in banded veins and around breccia fragments. Vugs are rare, but are more common in calcite than quartz veins. Up to twelve bands have been observed in some calcite veins.

Accessory gangue minerals consist of chlorite (\pm epidote) and hematite. Chlorite occurs as felty masses in quartz and calcite, typically as fine selvages along vein walls or between layers in banded veins. Chlorite is particularly abundant in high grade breccias, where it can form up to 20% of the gangue. Hematite is restricted to late calcite veins that are generally barren.

Cross-cutting veins and breccias attest to multiple episodes of fracturing

and infilling. Quartz-only veins formed early, in contrast to calcite-only veins, which always occur late in the sequence. Multi-stage veins typically show evidence of sequential filling of the fracture, beginning with fine-grained quartz at the vein wall, followed inwards by euhedral crystalline quartz, and medium to coarse grained calcite. At the transition from quartz to calcite, the two minerals are commonly intermixed and were evidently co-precipitated. Multi-stage breccias are typically composed of silicified wall-rock and quartz vein fragments cemented by quartz and calcite, or calcite alone. The bulk of the ore minerals, and therefore the highest ore grades, are hosted by the mixed quartz-calcite veins and breccias, and are commonly associated with abundant chlorite.

Ore Mineralogy

Ore minerals consist of pyrite, sphalerite, galena, chalcopyrite, acanthite, native silver and electrum, in order of decreasing abundance. Trace amounts of native gold have also been reported (Holbek, pers. com., 1989) but were not observed in this study. The ore minerals typically occur at vein margins and between vein bands, and particularly along the contacts between quartz and calcite zones in the mixed quartz-calcite veins and breccias (Fig. 9)

In hand specimens, the ore minerals are generally recognized as disseminated grey sulphides, commonly associated with pyrite and chlorite, and generally total less than 5% of the rock volume. High grade breccias, however, can contain up to 20% of pyrite and chlorite by volume, and return assay values

Figure 9. 9a) A reflected light photomicrograph of euhedral pyrite grains hosted by early crystalline quartz and later calcite
9b) A transmitted light photomicrograph of ore minerals (sphalerite+galena+acanthite) precipitated at the contact between early quartz and later calcite in a narrow veinlet. The wall-rock is at lower edge of the photograph. Quartz, closest to vein wall, displays rounded grains (Sample CK84-14 70 3, see Fig 15)

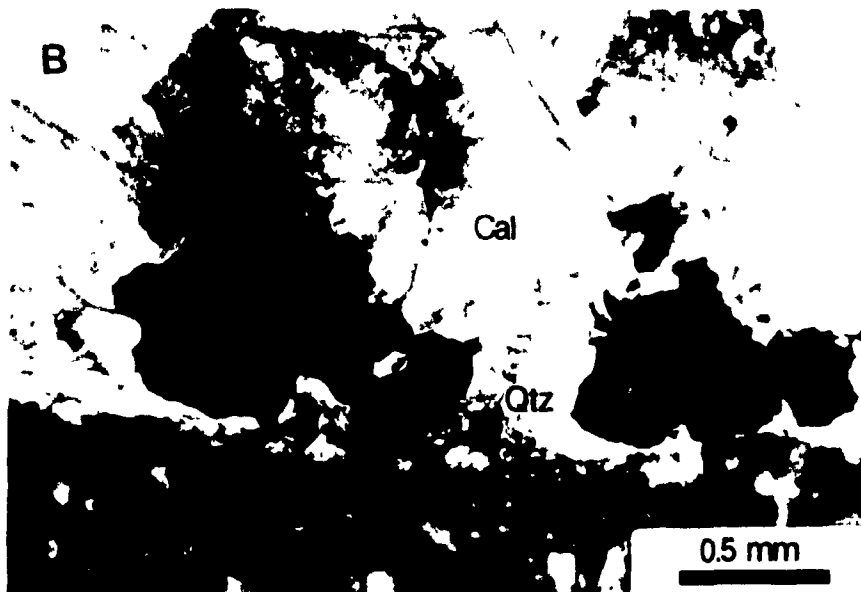
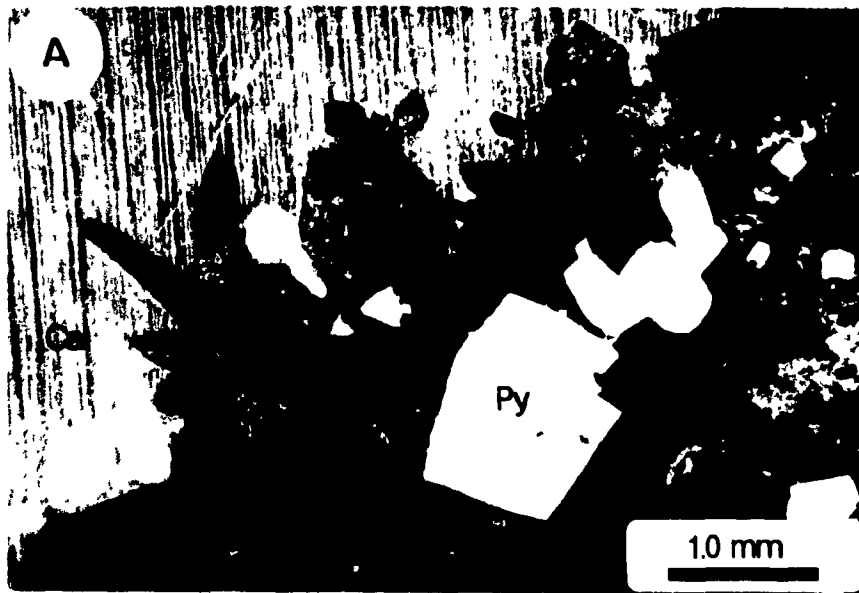
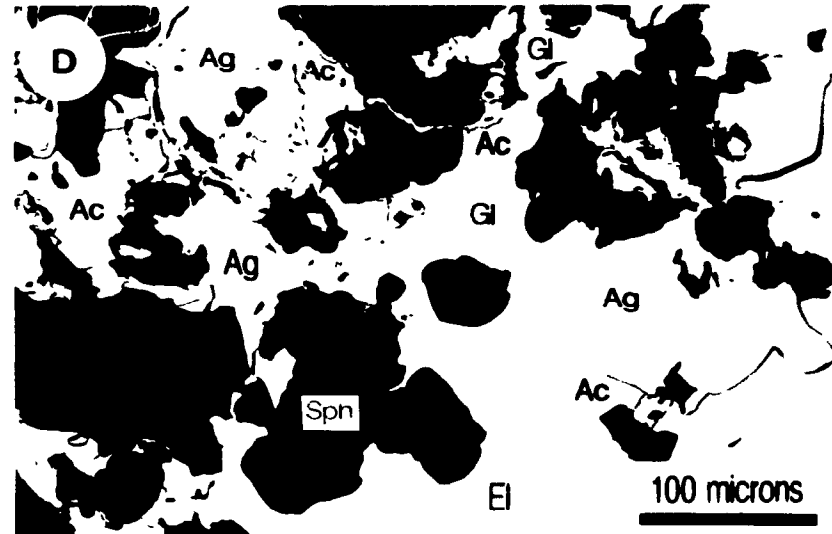
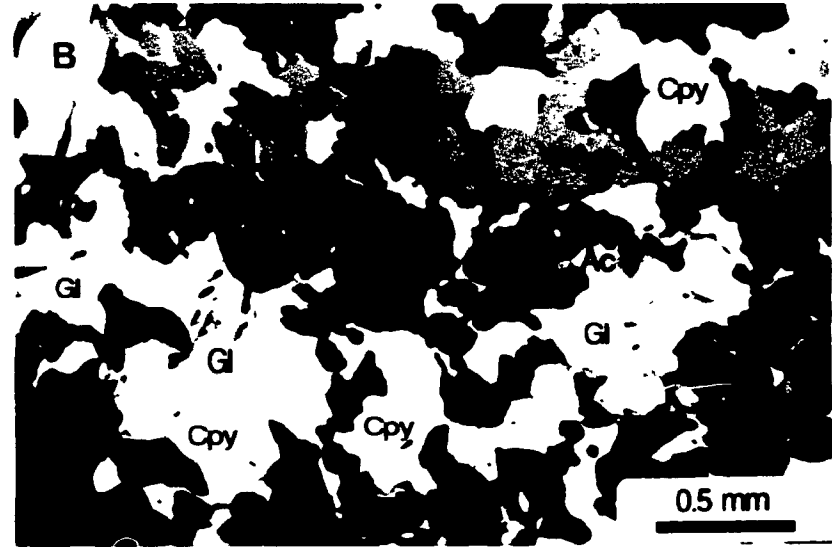
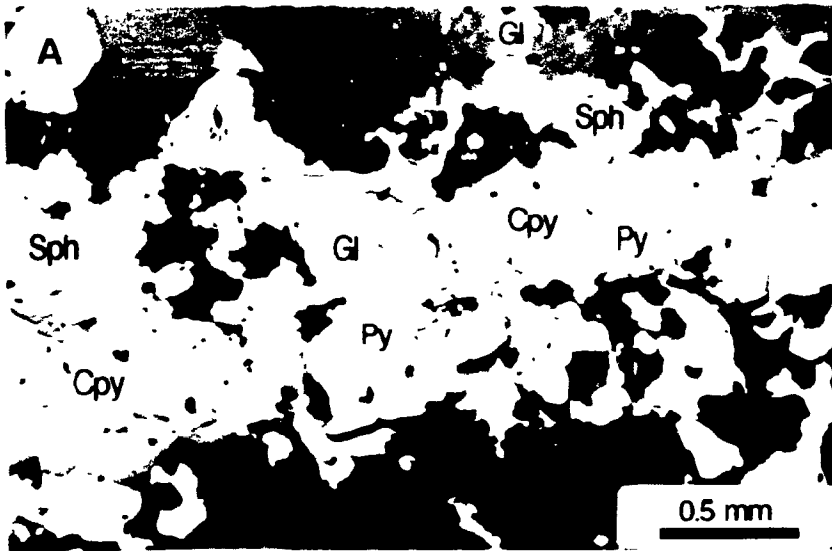


Figure 10. Photomicrographs showing typical ore mineral textures. 10a) Early euhedral pyrite, followed by sphalerite, chalcopyrite, and interstitial galena. 10b) Sphalerite followed by chalcopyrite, and galena coprecipitated with acanthite (right side of photo). 10c) Early pyrite, which has been fractured and embayed and infilled by galena, acanthite and electrum. 10d) Galena, acanthite, electrum and native silver precipitated after sphalerite. Photographs a,b,c are in reflected light; d is an SEM TV image.



as high as 345 g/t Au, 22,100 g/t Ag, plus several percent combined Cu, Pb and Zn.

Detailed petrographic studies indicate that the ore minerals are closely related in both spatial and temporal terms (Fig. 10) Pyrite was precipitated first and is hosted almost exclusively by early quartz. It was originally euhedral, but has been extensively fractured, pitted and embayed. Sphalerite and chalcopyrite were deposited next, as rounded to irregular grains in early quartz, interstitial to intermixed quartz and calcite, or filling fractures and embayments in earlier pyrite. Sphalerite is variably affected by "chalcopyrite disease", which is more pervasive where sphalerite and chalcopyrite are in direct contact. Quantitative analysis of sphalerite by electron microprobe showed it to be iron-poor, containing between 0-2 mol% Fe (Appendix III)

Galena, argentite (acanthite), electrum and native silver were then precipitated (in that order), interstitial to pyrite, sphalerite and chalcopyrite (Fig. 10), or in fractures in pyrite. These minerals are hosted predominantly by the mixed quartz-calcite phase of gangue mineral deposition, less so by late calcite, and never by early quartz. Galena and acanthite show a strong affinity and typically occur together, suggesting co-precipitation. Electrum occurs in contact with galena, acanthite and native silver, and less commonly as rounded, isolated grains. Native silver occurs interstitial to all other ore minerals and as irregular, isolated grains, particularly in calcite co-precipitated with quartz.

Individual electrum grains are commonly zoned, particularly where they

are in contact with native silver. Semi-quantitative analyses using a scanning electron microscope equipped with an energy dispersive system showed that some electrum grains have gold-rich cores (ave. 41% Au), and silver rich rims (ave. 14% Au) (Appendix III).

Paragenesis

It is significant that the ore minerals galena, acanthite, electrum and native silver occur primarily at the transition from quartz to calcite dominance, and are concentrated in multi-stage hydrothermal breccias. These and other relationships described above can be represented by a paragenetic sequence consisting of pre-ore, ore and post-ore stages (Fig. 11). In the pre-ore stage, euhedral pyrite was deposited in early quartz veins, with minor sphalerite and chalcopyrite. At the onset of ore deposition, the veins were reopened and/or brecciated, resulting in pyrite cataclasis, and the majority of sphalerite and chalcopyrite was deposited. During the ore stage, galena, acanthite, electrum and native silver were precipitated contemporaneously with quartz and calcite (\pm chlorite) in hydrothermal breccias. In the post-ore stage, minor amounts of hematite were deposited in generally barren calcite veins (Fig. 12).

FLUID INCLUSIONS

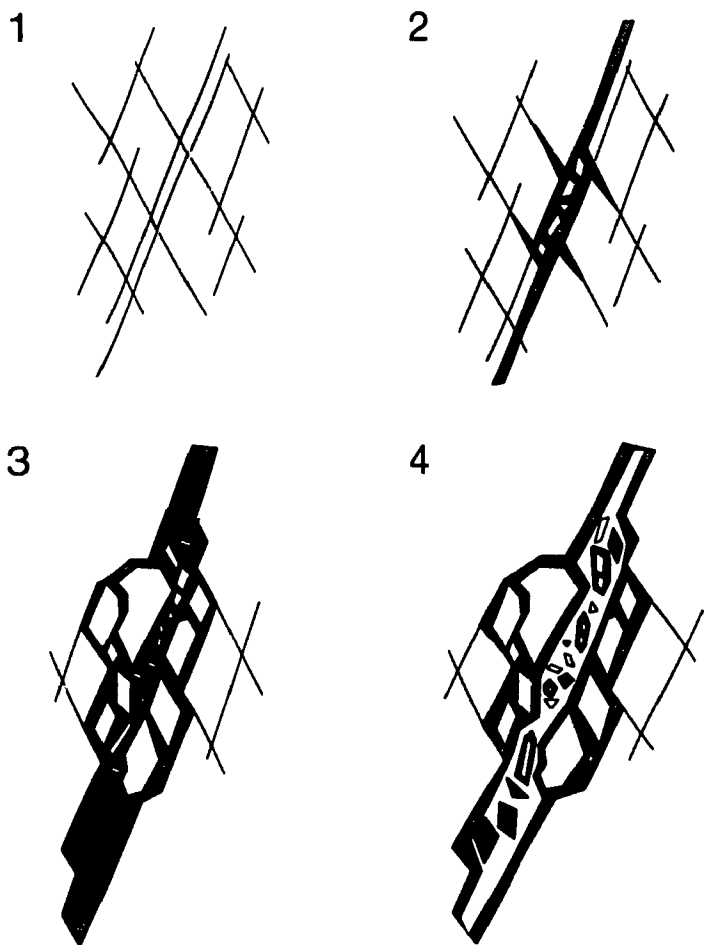
Petrography

Samples of ore stage quartz and calcite were selected for fluid inclusion

Figure 11. The paragenetic sequence of mineralization and alteration at Shasta.

STAGE	PRE-ORE	ORE	POST-ORE
MINERALIZATION	VEINS	BRECCIAS	VEINS
QUARTZ CALCITE CHLORITE HEMATITE PYRITE SPHALERITE CHALCOPYRITE GALENA ACANTHITE ELECTRUM NATIVE SILVER			
ALTERATION			
PROPYLITIC POTASSIC SERICITIC			

Figure 12. Schematic representation of typical ore-breccia formation at Shasta.



- 1 Potassic Alteration and Silicification
- 2 Pre-Ore Quartz Stockwork Veins
- 3 Ore Stage Quartz+Calcite Breccia
- 4 Post-Ore Calcite Vein

study, in order to "bracket" the transition from quartz to calcite dominance and constrain the physico-chemical conditions of ore deposition. Fluid inclusions suitable for analysis were identified in both minerals, except very early fine-grained quartz, which is turbid due to large numbers of 1-2 micron diameter inclusions. Turbidity also made some samples of later quartz and calcite unusable.

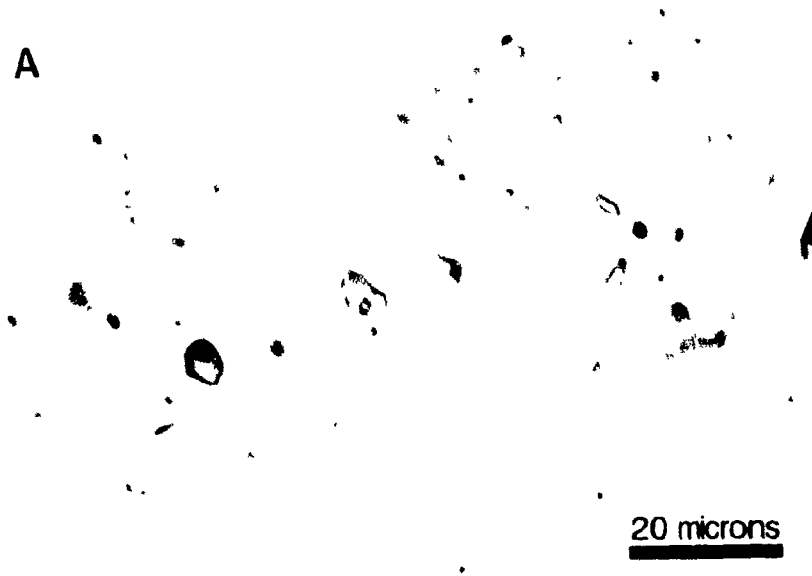
Three types of fluid inclusions were observed: liquid-vapour (L-V), liquid-only (L); and vapour-only (V). All inclusions were interpreted to be aqueous in nature, as neither carbonic liquids or clathrates were observed on cooling, and crushing tests resulted in vapour bubble collapse.

Liquid-vapour inclusions comprise about 50% of the total fluid inclusion population. The majority of quartz-hosted L-V inclusions are isolated but also occur in small three dimensional groups, away from crystal boundaries (Fig 13a). They are rounded to cusped in shape and average 3x5 microns in size. Calcite-hosted L-V inclusions typically occur as planar groups or linear trains, parallel to cleavage planes and crystal boundaries (Fig 13b). They display rod-shaped and negative crystal (rhombic) morphologies, and average 5x10 microns in size. Vapour to liquid phase ratios in L-V inclusions were calculated to range between 10-25% overall (Bodnar, 1983), but are more consistent ($\pm 5\%$) among close neighbours.

Liquid-only inclusions are relatively rare, and comprise less than 20% of the inclusion population. These inclusions occur mainly in quartz, and almost

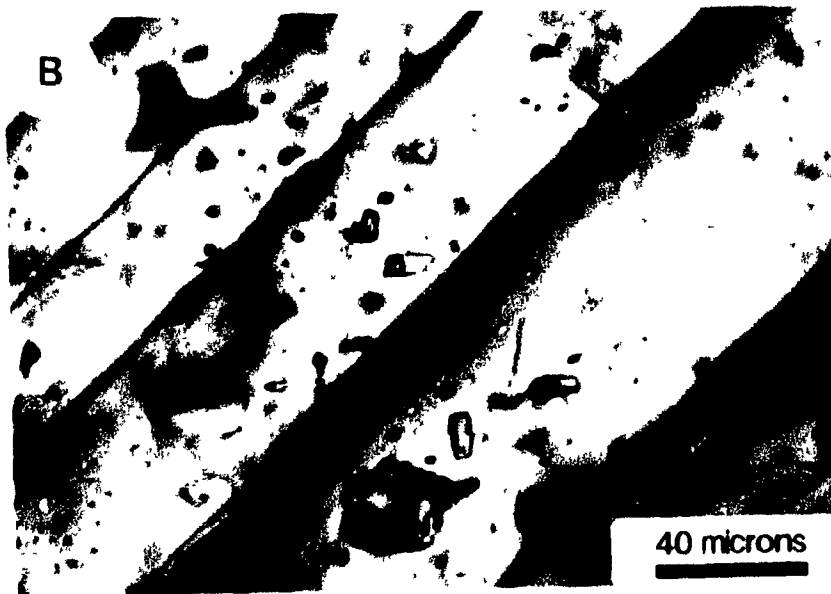
Figure 13. Photomicrographs of typical quartz-hosted inclusions (13a) and calcite-hosted inclusions (13b). Transmitted light.

A



20 microns

B



40 microns

exclusively in planar groups along variably healed fracture planes, with rare coexisting L-V inclusions. In quartz, liquid-only inclusions tend to be round and less than 2 microns in diameter, whereas in calcite, they are irregular to rhombic in shape and up to 10 microns across.

Vapour-only inclusions constitute the remaining 30% of the inclusion population. They occur mainly in calcite, almost exclusively along partially healed fractures and within cleavage planes, with rare L+V inclusions. Vapour-only inclusions are highly irregular in shape and size, ranging up to 30 microns across.

Origin

L-V inclusions that occur parallel to crystal boundaries in calcite are unambiguously primary in nature. Those that occur parallel to (but not within) cleavage planes are also considered to be primary. Liquid- and vapour-only inclusions that occur along obvious fracture planes or within cleavage planes are assumed to be secondary in nature. Rare L-V inclusions that coexist with L and V inclusions along fracture planes are probably the result of leakage or necking down and are also considered secondary.

L-V inclusions in quartz are less easily classified because of a lack of obvious primary features. However, these inclusions display relatively consistent vapour/liquid ratios, which indicates that leakage and necking-down have not been significant. In one case where unequivocally primary inclusions were

observed in a crystal growth zone, the inclusions had vapour to liquid ratios similar to the isolated inclusions. This suggests that the isolated L-V inclusions in quartz are probably primary.

Microthermometry

Microthermometric analyses were conducted on primary and secondary liquid-vapour inclusions in samples from mineralized zones, using a Fluid Inc - USGS modified gas-flow heating and freezing stage (Werre et al., 1979). Calibration was achieved using synthetic aqueous inclusions, and measurements were accurate to $\pm 0.2^\circ\text{C}$ for subzero temperatures and $\pm 2.0^\circ\text{C}$ at the highest temperatures to which samples were heated.

During heating runs, all inclusions homogenized to liquid between 130°C and 310°C . Histograms of homogenization temperatures (T_h , $^\circ\text{C}$) (Fig. 14) show that quartz-hosted inclusions have a dominant T_h peak centred at 280°C , with a spike at 295°C , and a subordinate T_h peak at 220°C . Calcite-hosted inclusions have a dominant T_h peak at 275°C , a subordinate T_h peak at 225°C , and a minor T_h peak at 195°C .

Microthermometric traverses across two 1 cm wide veinlets (Fig. 15) displayed similar progressions of decreasing T_h from early quartz to later calcite. Inclusions in quartz, closest to the vein wall, homogenized between 290°C and 250°C , whereas inclusions in calcite homogenized between 260°C and 190°C , decreasing towards the vein centre.

Figure 14. Histograms of fluid inclusion microthermometric data and calculated fluid salinities for samples from mineralized zones (Oakes et al , 1990). T_h is the homogenization temperature; T_e is the eutectic or initial ice melting temperature; T_m ice is the final ice melting temperature.

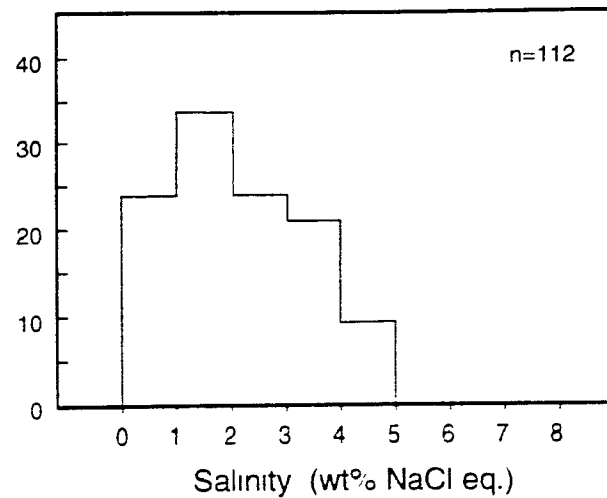
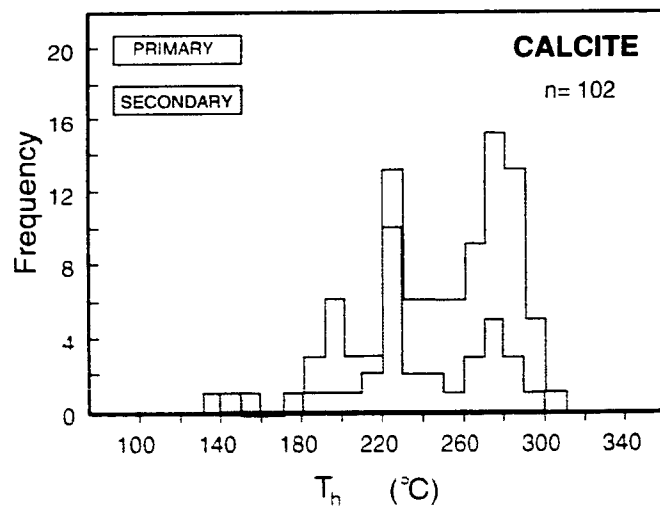
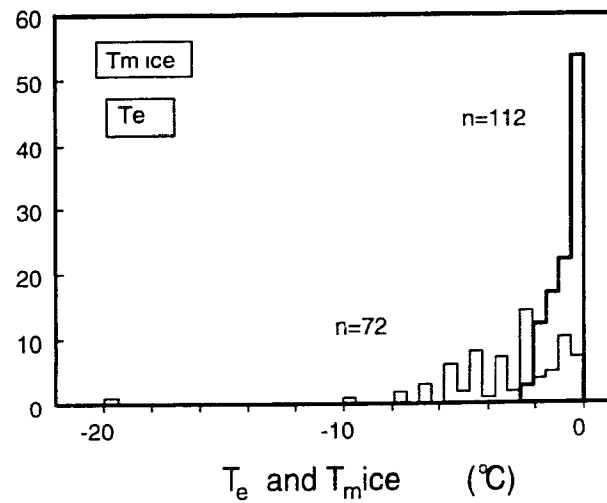
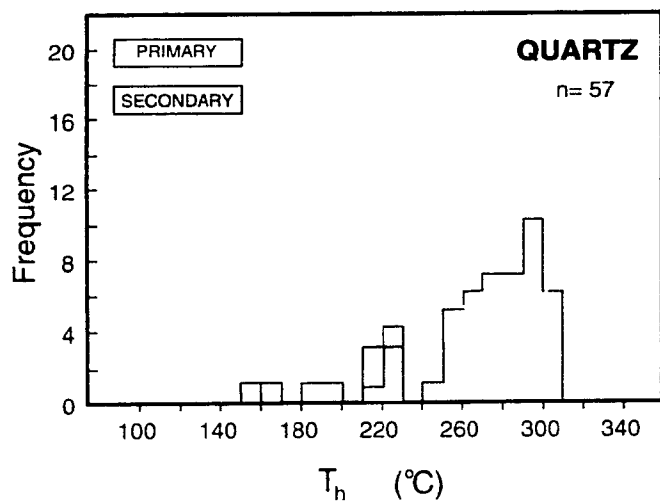
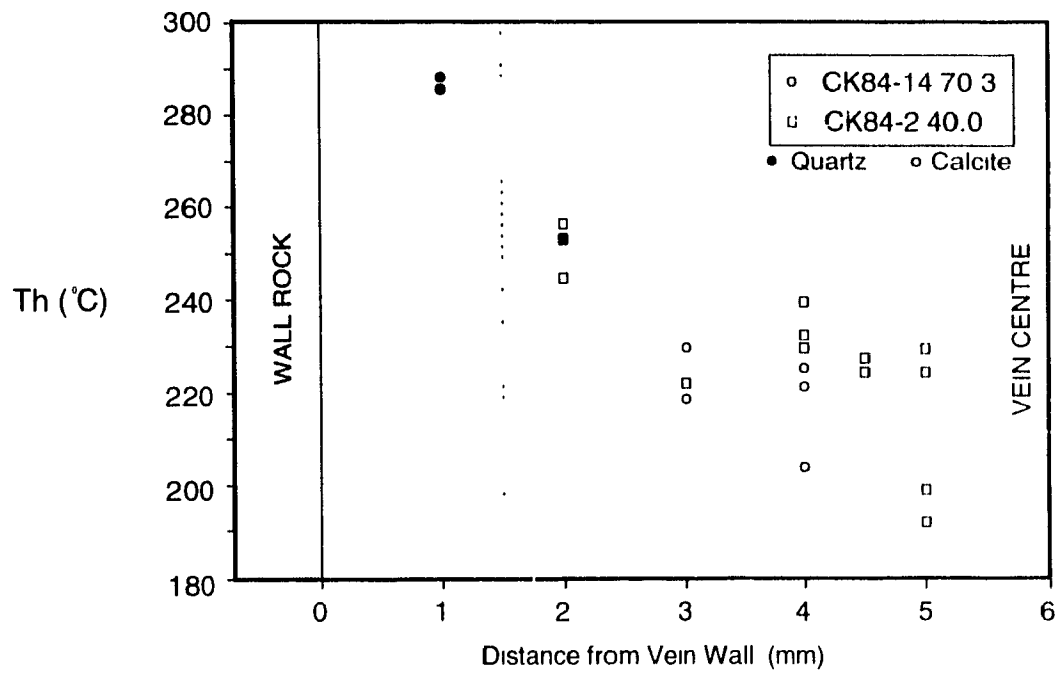


Figure 15. The distribution of T_h for L-V inclusions across two narrow veinlets in the Creek zone. The dotted line represents mineralization in sample CK84-14 70.3, (see Fig. 9b).



On cooling, inclusions froze routinely at about -40°C , but ice was never visible, due to the similar refractive indices of the ice and quartz. Eutectic melting temperatures (T_e) were therefore very difficult to measure, as melting was observed only as very subtle growth or movement of the vapour bubble. Initial indications of melting were typically observed at temperatures above -9°C (Fig. 14). The lowest temperature at which bubble movement was noted was approximately -20°C .

Final melting temperatures (T_m ice) are tightly bracketed between -2°C and 0°C , and there is no significant difference in the temperatures for quartz- and calcite-hosted inclusions. Calculated values of fluid salinity, using the equation of Oakes et al (1990) vary between 0 and 5 weight percent NaCl equivalent, with a peak between 1-2 wt% NaCl eq. (Fig. 14).

Decrepitate Analyses

Three samples of quartz from ore stage quartz-calcite veins were chosen for fluid inclusion decrepitate analyses (Haynes et al., 1988) in order to determine the composition of the hydrothermal fluid. Decrepitate residues (Fig. 16) were produced by heating clean fluid inclusion sections to roughly 400°C to decrepitate the inclusions. The residues were then analyzed semi-quantitatively using a scanning electron microscope equipped with an energy dispersive X-ray spectrometer, set to wide raster mode.

The only elements detected in the residues were Na, K, Ca, Cl and S,

which are present in an average weight ratio of 5.3 2 9.1 (Table 1) Using the average salinity of L-V inclusions (2 wt % NaCl eq. or 0.4m), it is estimated that the hydrothermal fluid contained approximately 0.26m Na, 0.1m K, 0.04m Ca and 0.01m S. Charge balance calculations indicate that cationic charge exceeds anionic charge by about 20%, which may be due to the semi-quantitative nature of the decrepitate analyses, or to undetected carbon in the form of CO_3^{2-} or HCO_3^- .

CHLORITE GEOTHERMOMETRY

Independent estimates of the temperature of ore deposition were obtained using the chlorite geothermometer of Cathelineau (1988). Temperatures are calculated using the empirical relationship between temperature and the Al content in the tetrahedral site of the chlorite, determined by electron microprobe analyses (Appendix III). Samples tested consisted of vein material containing chlorite that occurs at the contact between pre-ore quartz and ore stage quartz-calcite, and therefore represents the transition from quartz to calcite dominance. The results of seven analyses give an average temperature of $262 \pm 5^\circ\text{C}$, which is in excellent agreement with the temperatures estimated from fluid inclusion microthermometry ($280^\circ\text{-}225^\circ\text{C}$).

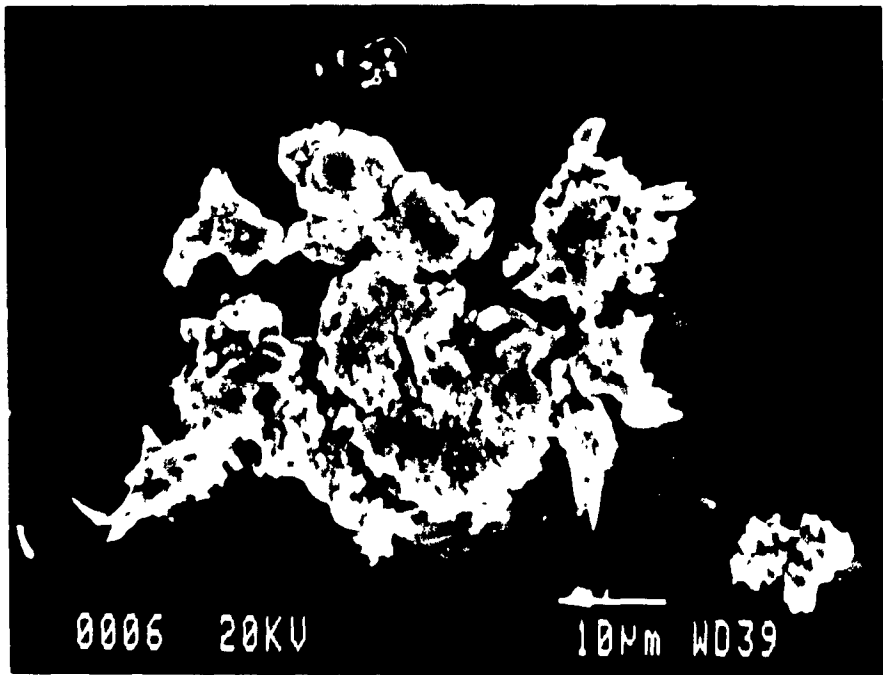
Table 1 Fluid Inclusion Decrepitate Data (wt%).

Table 1 Fluid Inclusion Decrepitate Data (wt%)

	Na	Ca	K	Cl	S
JM87-23	28 76	0 00	12 76	58 48	0 00
	30 69	0 00	0 00	69 31	0 00
	33 29	19 90	12 45	34 36	0 0
	29 67	13 18	8 78	35 57	12 81
	36 82	0 00	0 00	62 02	1 16
	19 48	1 56	26 15	51 58	1 23
	39 90	6 01	0 00	50 71	3 38
CK89-04	23 84	4 46	21 24	42 26	8 21
	22 74	9 44	13 59	41 66	12 56
	20 92	11 83	22 39	35 99	8 88
	12 20	18 12	20 89	41 08	7 71
	14 75	13 02	25 62	40 55	6 06
	14 10	18 70	23 08	37 05	7 07
JM 87-11	22 83	5 63	23 90	47 6	0 00
	20 86	8 03	15 90	46 4	8 88
	20 96	12 32	19 50	43 01	4 22
	26 67	9 16	16 30	44 02	3 84
	37 62	21 47	8 70	32 22	0 00
	22 92	6 22	28 05	38 66	4 15
<hr/>					
Average (wt%)	Na	Ca	K	Cl	S
	25 21	9 42	15 75	44 87	4 75
<hr/>					
Average (at%)	Na	Ca	K	Cl	S
	34 01	7 35	12 50	39 52	6 6
<hr/>					
Atomic Ratios	Na/Cl	Ca/Na	K/Na	Al/Cl	S/Cl
	0 86	0 22	0 37	1 36	0 17
<hr/>					
Molal Concentration*	Na	Ca	K	S	
	0 26	0 06	0 1	0 01	

* Estimated assuming 2wt% Na eq = 0 4m

Figure 16 Microphotograph of a typical fluid inclusion decrepitate observed in this study. Bladed crystals are KCl, groundmass is NaCl and CaCl₂.



0006 20KV

10µm WD39

STABLE ISOTOPES

Sulphur

Analyses of sulphur isotopic composition were performed on samples of country rock and sulphide mineralization in an effort to identify the source of sulphur in the hydrothermal system, and to examine the evolution of the mineralizing fluid with respect to fO_2 and pH conditions

The sulphide samples were chosen to represent a "cross-section" of mineralization from pre-ore and ore stage veins and breccias. The samples consisted mainly of hand picked mineral separates of pyrite because of its ease of separation, other sulphide minerals were so intimately associated that they could not be mechanically separated. Nevertheless, two composite samples of especially high grade mineralization consisting of sphalerite, galena and acanthite (\pm electrum) were also chosen for study. Country rock samples consisted of drill core assay pulps, representing unmineralized bulk samples of feldspar-quartz lapilli tuff. Analyses were conducted at the University of Saskatchewan Isotope Laboratory and are accurate to within 0.1 ‰. Sulphur isotope compositions are reported in standard δ notation, relative to the Cañon Diablo troilite.

The isotopic compositions and the corresponding gold-silver grades of the pyrite samples are reported in Table 2. The $\delta^{34}S$ values for country rock pyrite average -1.6 ± 0.9 ‰, whereas vein pyrite $\delta^{34}S$ values range from -3.4 to -5.7 ‰, and the two composite samples had $\delta^{34}S$ values of -5.4 and -7.3 ‰. It is

Table 2. Sulphur Isotope Data

Table 2 Sulphur Isotope Data

Sample	Grade Au/Ag (g/t)	Measured $\delta^{34}\text{S}$ (‰)	Calculated ² $\delta^{34}\text{S}_{\text{H}_2\text{S}}$ (‰) 280°C	225°C
Pyrite Separates				
CREEK ¹	14.6 / 134.0	-3.4	-4.7	-5.0
JMTC5-3	0.6 / 55.5	-3.5	-4.8	-5.1
CRK-1 ¹	1.9 / 61.5	-3.8	-5.1	-5.4
JMHG-PT	71.1 / 7271.7	-4.7	-6.0	-6.3
JMPTHG-D1	345.0 / 22,100.0	-5.0	-6.3	-6.6
JMPTHG-D2	225.9 / 88,374.0	-5.6	-6.9	-7.2
JMHGTR-B	9.4 / 371.0	-5.7	-7.0	-7.3
Composites				
JMPT-CBV	1015.0 / 17,518.0 (70% ZnS, 24% PbS, 6% Ag ₂ S)	-5.4	-5.0	-4.9
JMPTHG-D2	225.9 / 88,374.0 (34% ZnS, 36% PbS, 30% Ag ₂ S)	-7.3	-5.9	-5.6
Bulk Country Rock				
8-1 42.5	barren	-0.7		
8-31 25.7	02 / 1.0	-2.5		
8-31 25.7	duplicate	-2.5		

1 Quartz-hosted mineralization

2 Calculations based on the equations of Ohmoto and Rye (1979)

significant that the $\delta^{34}\text{S}$ values for vein pyrite are lower than those for country rock pyrite. This trend to lower $\delta^{34}\text{S}$ values may reflect increases in the $f\text{O}_2$ - pH conditions of the fluid, which will be examined in greater detail in a later section.

$\delta^{34}\text{S}_{\text{H}_2\text{S}}$ values for a hydrothermal fluid in equilibrium with the sulphide samples were calculated at 280°C and 225°C (corresponding to the T_{H} peaks indicated by fluid inclusion microthermometry) using the appropriate fractionation equations of Ohmoto and Rye (1979). In the case of the composite samples, $\delta^{34}\text{S}_{\text{H}_2\text{S}}$ was calculated from the combined fractionation of sphalerite, galena and acanthite with H_2S , weighted according to the proportions of these minerals in the samples. The latter were estimated semi-quantitatively from scanning electron microscope X-ray images of Zn, Pb and Ag. Calculated $\delta^{34}\text{S}_{\text{pyrite}}$ values for pyrite separates decrease from -4.7 to -7.0‰ (at 280°C) as gold-silver assays increase from sub-economic to ore grades. The values of $\delta^{34}\text{S}_{\text{pyrite}}$ calculated for the composite samples are -5.0 and -5.9‰, for the lower and higher grade samples respectively.

Oxygen and Deuterium

Analyses of oxygen and deuterium isotopic composition were conducted on samples of vein and breccia gangue minerals to determine the provenance of the mineralizing fluid. All samples consisted of hand-picked mineral separates from ore stage veins and breccias. Oxygen isotope analyses were conducted on separates of quartz, calcite and chlorite, whereas hydrogen isotope analyses

Table 3. Oxygen and Hydrogen Isotope Data.

Table 3 Oxygen and Hydrogen Isotope Data

Sample	Measured $\delta^{18}\text{O}$ (‰)			Calculated ¹ $\delta^{18}\text{O}_{\text{fluid}}$ (‰)		
	Qtz	Cal	Chl	280°C		225°C
JMHGPT	6.4	3.6		-1.2	-2.6	-4.7
CBVEIN	6.0	3.9		-1.6	-2.3	-4.4
HGTR-B		4.0			-2.2	-4.3
84-14-72 3		5.7			-0.5	-2.6
89-12-48 5	5.3			-2.3		
84-12-60 4	6.5			-1.1		
CBV-CHL2			6.1			-4.6 ³
Average	6.1	4.3		-1.6	-1.9	-4.1

Sample	Mineral	Measured δD (‰)	$\delta\text{D}_{\text{fluid}}$ (‰)
89-12-48 5	Qtz	-148 ³	-148
84-12-60 4	Qtz	-171 ³	-171
CBV-CHL1	Chl	-102	-152 ³
CBV-CHL2	Chl	-112	-162 ³
Average			-158

1 Calculated using the equations of Matsuhisa et al (1979) for quartz, Friedman and O'Neil (1977) for calcite

2 Based on the empirical curves of Taylor (1979) at 280°C

3 Measured directly from crushed fluid inclusions

were performed on chlorite separates and the fluid released from inclusions in quartz separates. Analyses were conducted at the University of Saskatchewan Isotope Laboratory and are accurate to within 0.1 ‰. Oxygen and hydrogen isotopic compositions are reported in standard δ notation, relative to Standard Mean Ocean Water (Craig, 1961) in Table 3.

$\delta^{18}\text{O}$ values for quartz are well constrained about an average of $6.1 \pm 0.5\text{‰}$, whereas those of calcite are slightly lower at $4.3 \pm 1.4\text{‰}$. A single chlorite sample yielded a $\delta^{18}\text{O}$ value of 6.1‰ . The average $\delta^{18}\text{O}_{\text{fluid}}$ values for a hydrothermal fluid in equilibrium with these samples were calculated to be -1.6‰ from quartz and -1.9‰ from calcite at 280°C , and -4.1‰ from calcite at 225°C (consistent with the T_h peaks indicated for L-V fluid inclusions) using the equations of Matsuhisa et al. (1979), and Friedman and O'Neil (1977), respectively.

The measured δD values of the quartz samples are -148‰ and -171‰ . These are assumed to be equivalent to $\delta\text{D}_{\text{fluid}}$, since the principal source of hydrogen is water released from inclusions that are interpreted to represent the original hydrothermal fluid. The measured δD values for chlorite are -102‰ and -112‰ . $\delta\text{D}_{\text{fluid}}$ values calculated for a fluid in equilibrium with the chlorite samples are -152‰ and -162‰ , using the empirically derived fractionation factors of Taylor (1979). These values lie well within the range of values determined directly from fluid inclusions in quartz. The average value of $\delta\text{D}_{\text{fluid}}$ obtained from the combined data sets is -158‰ .

DISCUSSION

As previously noted, ore grade silver-gold mineralization at Shasta was deposited at the onset of calcite precipitation in veins and breccias. The occurrence of multi-stage, quartz-calcite hydrothermal breccias is strong evidence for boiling of the mineralizing fluid, as is the fine-grained nature of early quartz and the abundance of vapour-only inclusions, with coexisting L-V inclusions, observed in later calcite. The deposition of chalcedonic quartz indicates supersaturation of SiO_2 , and implies a sharp drop in temperature that could have been caused by adiabatic expansion of the boiling fluid. It is therefore reasonable to conclude that the hydrothermal system boiled at a relatively early stage, and continued to boil episodically at least until after the ore minerals had been deposited. Accordingly, any discussion of the genesis of the deposit needs to start by considering the hypothesis that boiling was also responsible for ore mineralization.

P-T Conditions

Evidence that the fluid boiled permits the homogenization temperatures of L-V inclusions to be used to estimate the depositional temperature directly. These data (Figs. 14 and 15) show clearly that the temperature was at a maximum in the pre-ore quartz stage (295°C), and decreased through the ore stage from 280 to 225°C . Similar temperatures ($262 \pm 5^\circ\text{C}$) were calculated using the chlorite geothermometer of Cathelineau (1988).

The initial ore stage temperature of 280°C corresponds to a fluid pressure of approximately 64 bars, based on the liquid-vapour curve of Haas (1971). This is equivalent to hydrostatic depth of about 750 m (for an aqueous solution containing 2 wt% NaCl equivalent, see below) or a lithostatic depth of 275 m. The former represents the maximum paleo-depth for ore grade mineralization at Shasta. The development of hydrothermal breccias indicates that the fluid pressure locally exceeded lithostatic pressure. This was probably due to local sealing of the hydrothermal conduit by early quartz deposition and was likely restricted to higher levels in the system (closer to 275m).

The above estimates of temperature and pressure indicate that the Shasta deposit formed under P-T conditions within the range typical of most epithermal deposits (100°-300°C; <1000 m).

Fluid Source

The oxygen and hydrogen isotopic compositions estimated for the ore fluid (Table 3) are most reasonably explained by meteoric waters that evolved through interaction with the volcanic rocks that host the deposit. The δD values are much lower than those characteristic of magmatic or metamorphic fluids (Fig. 17), but are similar to those of meteoric waters from high latitudes or elevation. The $\delta^{18}O$ values, although also lower than those of magmatic or metamorphic fluids, display a significant positive shift away from the Meteoric Water Line (Fig. 17). We attribute this to extensive interaction with isotopically heavier volcanic

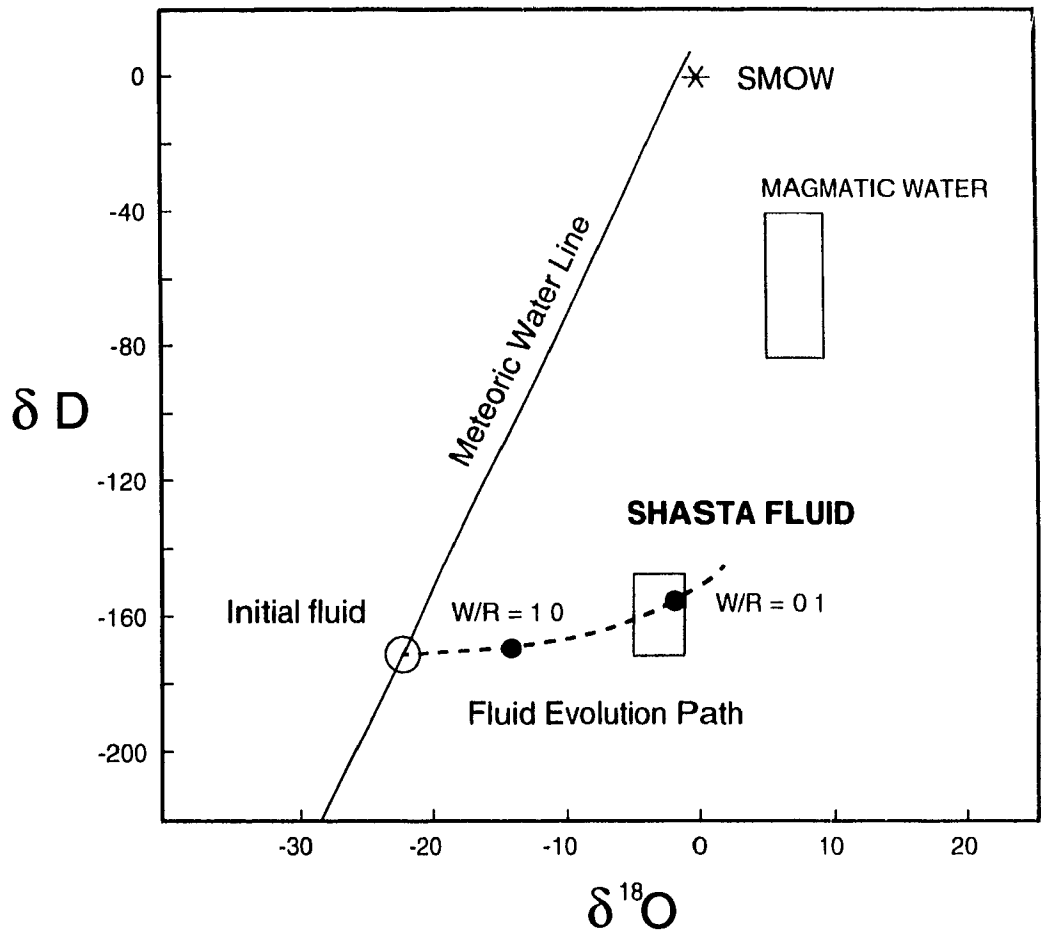
wall-rocks. This isotopic evidence for a dominantly meteoric ore fluid is also supported by the very low salinity of L-V inclusions (1-5 wt% NaCl eq).

The proposed modification of $\delta^{18}\text{O}_{\text{fluid}}$ as a result of fluid/rock interaction was investigated further by calculating water/rock ratios (W/R) using the equations of Ohmoto and Rye (1974). These calculations assumed that the fluid had initial $\delta^{18}\text{O}$ and δD values of about -22‰ and -165‰, respectively, propylitically altered volcanics had $\delta^{18}\text{O}$ and δD values of -9‰ and -70‰, respectively (Diakow et al., 1991; Field and Fifarek, 1985), and the fluid changed its composition by equilibrating with host rock feldspar (O'Neil and Taylor, 1967) and chlorite (Taylor, 1979). The assumed initial $\delta^{18}\text{O}$ and δD values of the fluid correspond to those of meteoric waters currently found in this part of British Columbia (Taylor, 1979). Although the deposit is Jurassic in age (Clark and Williams-Jones, 1990) and the host rocks are part of an allochthonous terrane, it is likely that the elevation and latitude of deposition were not greater than that of the Toadogone today. For simplicity, we have therefore assumed that the isotopic composition of the local meteoric water has not changed significantly since the Jurassic.

The water/rock ratio and possible path of isotopic evolution of the fluid are shown in Fig. 17. The former has a value of 0.1 at both 280°C and 225°C, using the average $\delta^{18}\text{O}_{\text{fluid}}$ and $\delta\text{D}_{\text{fluid}}$ values calculated from quartz and calcite in Table 3.

The above ratio is lower than those estimated for many epithermal

Figure 17. A plot of δD vs $\delta^{18}O$ showing the estimated composition of the Shasta fluid and water/rock ratio. The latter was calculated assuming the fluid was of meteoric origin and was isotopically modified as a result of interaction with surrounding volcanic wall rocks.



deposits in the Basin and Range province of the Western United States (>0.5); notable exceptions are the Bodie and Tonopah deposits, for which W/R ratios were estimated to be 0.01 and 0.2, respectively, (Field and Fifarek, 1985). It should be noted however, that boiling tends to enrich $\delta^{18}\text{O}_{\text{fluid}}$ and $\delta\text{D}_{\text{fluid}}$ values (Field and Fifarek, 1985), and thus the W/R ratios at Shasta may have been somewhat higher than those interpreted above.

Source of Sulphur and Metals

The most likely source of sulphur is the volcanic country rocks, which could have been scavenged for sulphur and ore metals by the circulating hydrothermal fluid. As discussed below, the interpreted $\Sigma\delta^{34}\text{S}_{\text{fluid}}$ (-1.6‰ , the average $\delta^{34}\text{S}$ of bulk country rock) and the $\delta^{34}\text{S}_{\text{H}_2\text{S}}$ values calculated from vein pyrite (-4.7 to -7.0‰) (Table 2) are both consistent with a magmatic (i.e. volcanic) source of sulphur (Field and Fifarek, 1985).

Propylitically altered country rocks (Toodoggone and Stuhini) were probably also the main source of silica, calcium and potassium. Underlying limestones of the Asitka Group, or interbedded limestones of the Stuhini Group may have provided an additional source of calcium, and this could account, in part, for the atypical, calcite-rich nature of the Shasta deposit.

Subvolcanic Omineca intrusives are considered to be the most likely source of the heat that was required to drive the Shasta hydrothermal system, and through this association, may have supplied some of the sulphur, and base

and precious metals.

fO₂-pH Conditions

Changes in fO₂ and pH are commonly invoked as causes of mineral deposition in hydrothermal systems. In order to investigate the possible role of these parameters in controlling Ag-Au mineralization at Shasta, we have constructed log fO₂ - pH diagrams (Figs 17-19) at 280°C and 225°C (representing the range of ore deposition temperatures), that show the initial conditions and interpreted evolution of the hydrothermal fluid.

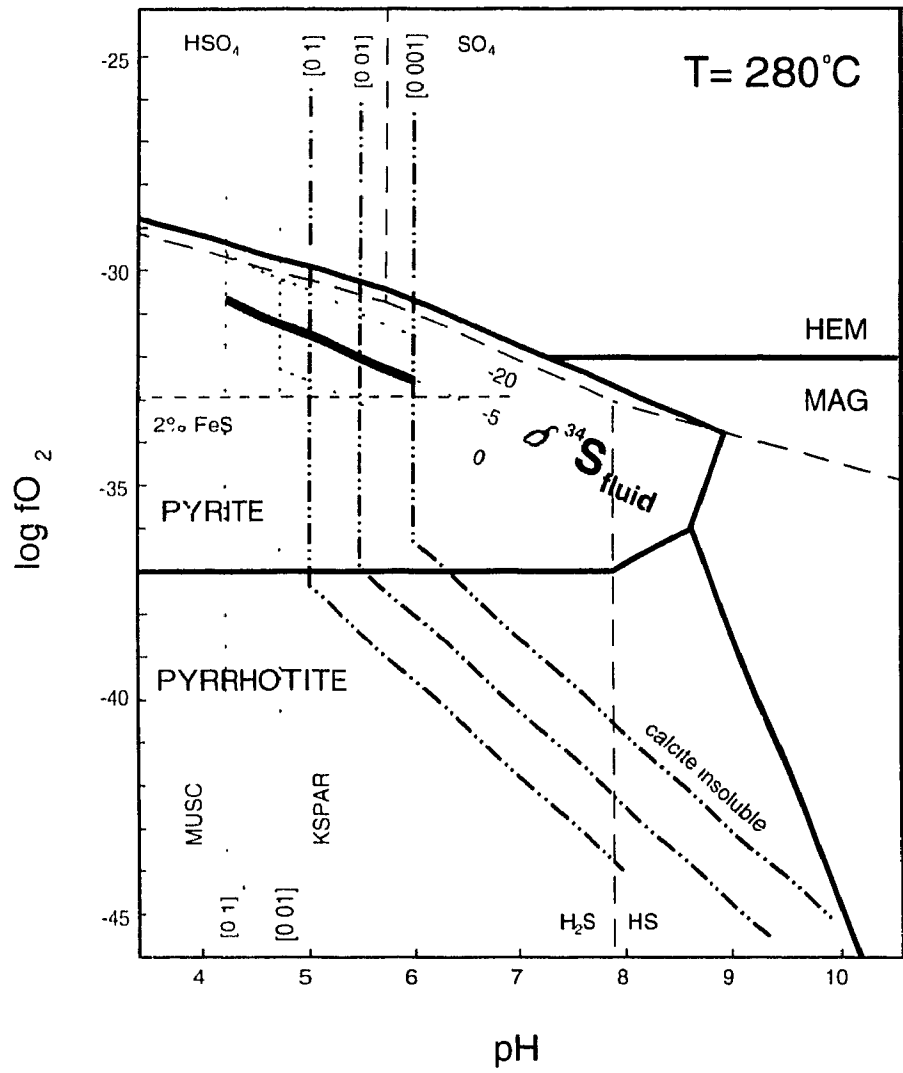
The concentrations of the various fluid components, which helped control the phase and species boundaries shown in the diagrams, were estimated mainly from the fluid inclusion decrepitate analyses discussed previously. These data indicate that potassium, calcium and sulphur concentrations were on the order of 0.1 *m*, 0.04 *m*, and 0.01 *m*, respectively. The carbon concentration, which is needed to determine the solubility of calcite, was below the detection limits of the decrepitate analyses. The lack of graphite in the deposit requires that it was less than about 0.01 *m* (Ohmoto, 1972), we have assumed a carbon concentration of 0.001 *m*. Predominance boundaries for sulphur species, the K-feldspar/muscovite phase boundary, the stability fields of the iron oxide and sulphide minerals, and the saturation boundary of calcite, were all calculated using the computer program SUPCRIT92 (Johnson et al., 1991). Silver mineral stability fields were calculated using the data of Gammons and Barnes (1989),

and the contours of $\delta^{34}\text{S}_{\text{H}_2\text{S}}$ from the data of Ohmoto (1972) The saturation limit for calcite and stability boundary for K-feldspar/muscovite are shown at several concentrations of potassium and carbon for comparative purposes.

An estimate of the initial log $f\text{O}_2$ -pH conditions of the ore fluid at the inception of boiling at 280°C is represented by the shaded area in Fig. 18. The initial pH is constrained, by the occurrence of potassic alteration and the lack of calcite, to have been between 4.25 (the pH of K-feldspar-muscovite equilibrium) and 6 (the pH of calcite saturation) These conditions are consistent with the occurrence of pyrite in the pre-ore mineral assemblage. The upper and lower limits of log $f\text{O}_2$ values are constrained by the pyrite-hematite boundary and the FeS content of sphalerite (0-2% atomic) (Scott and Barnes, 1971), to have been -30 and -33, respectively

Further constraints on the probable initial log $f\text{O}_2$ - pH conditions are provided by the $\delta^{34}\text{S}$ data for pyrite (Table 2), which suggest that $\delta^{34}\text{S}_{\text{H}_2\text{S}}$ values ranged from -4.7 to -7.0 ‰ at 280°C. The value of -4.7‰ is assumed to reflect the composition of H_2S in the fluid at the onset of ore deposition. This value, when compared with the contours for $\delta^{34}\text{S}_{\text{H}_2\text{S}}$ shown in Fig. 18 (based on the assumption that $\Sigma^{34}\text{S}_{\text{fluid}} = -1.6\text{‰}$, the average $\delta^{34}\text{S}$ of the host volcanics) indicates that log $f\text{O}_2$ and pH were in the range of -30.5 to -32.5 and 4.25 to 6, respectively

Figure 18. Log fO_2 - pH diagram constructed at 280°C, showing the predominance fields for aqueous sulphur species, and stability fields for minerals in the Fe-S-O system, K-feldspar-muscovite and calcite $\Sigma[S]= 0.01m$, $[K]= 0.1m$, and $I= 0.5$ based on decrepitate and microthermometric data $\Sigma[C]= 0.001m$, is an assumed value (see text for more detail). Thermodynamic calculations were performed using the computer program SUPCRIT92 (Johnson et al., 1992). Contours of $\delta^{34}S_{H_2S}$ were calculated using the data of Ohmoto (1972) and an assumption that $\Sigma\delta^{34}S=0$. The horizontal "2% FeS" line in the pyrite field reflects the iron content in sphalerite. The shaded area represents the probable initial fluid conditions, discussed in the text. The thick contour line represents the range in pH and log fO_2 conditions constrained by $\delta^{34}S_{H_2S}$ values.



Fluid Evolution

The observed mineral paragenesis displays a progression from pre-ore quartz and pyrite, to ore stage quartz-calcite and silver-gold mineralization, to post-ore calcite (\pm hematite). Within the ore stage itself, there was a progression from early acanthite to later electrum and native silver. These changes in mineralogy, i.e. from calcite undersaturation to saturation, from acanthite to native silver, and pyrite to hematite stability, require a corresponding evolution of the fluid to higher pH (Figs 18 and 19). Whether or not there was also an increase in fO_2 cannot be established from these data. However, the previously mentioned trend of $\delta^{34}S_{H_2S}$ to lower values with increasing ore grade (Table 2) is strong evidence that both fO_2 and pH increased. Significantly, these increases are predicted consequences of boiling, pH and fO_2 increase due to loss of CO_2 and H_2 to the vapour phase, respectively (Drummond and Ohmoto, 1985).

Ore Transport and Deposition Controls

Seward (1976), Shenberger and Barnes (1989), and Hayashi and Ohmoto (1991) have shown that gold is most efficiently transported as a bisulphide complex in most epithermal environments. The most common bisulphide species is $Au(HS)_2^-$ (Shenberger and Barnes, 1989), although Hayashi and Ohmoto (1991) have shown that the $HAu(HS)_2$ species is also important below pH=5.5. Chloride complexing of gold predominates only at temperatures above 300°C, or if the fluid is unusually H_2S poor and chloride-rich, (conditions

Figure 19. Log fO_2 - pH diagrams constructed at 280°C and 225°C, under the same conditions as Fig 18, showing gold solubility contours calculated using the data of Seward (1973).

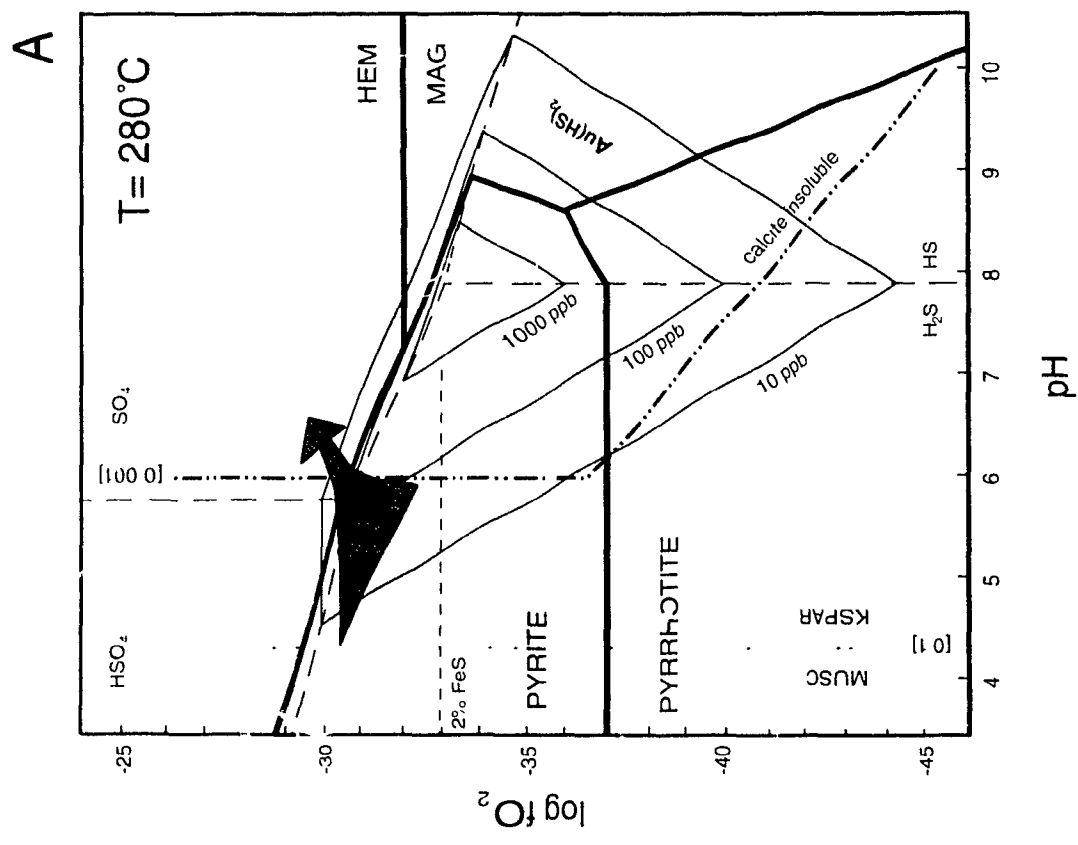
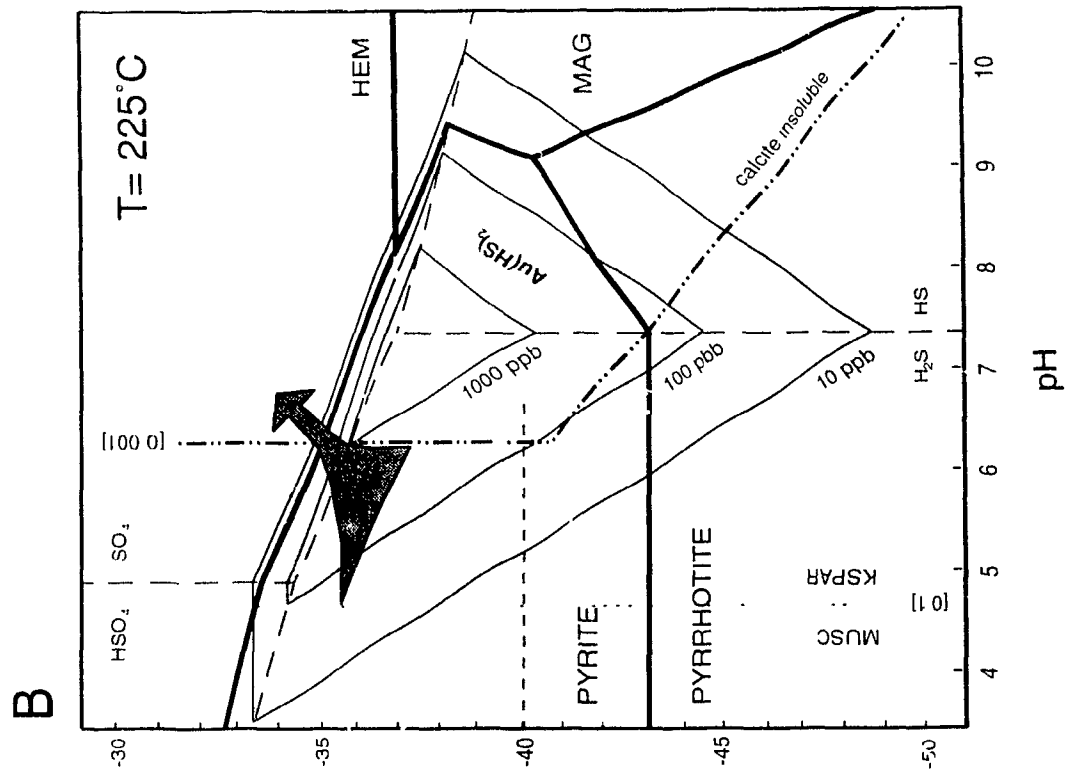


Figure 20. Log fO_2 - pH diagrams constructed at 280°C and 225°C, under the same conditions as in Fig 18, showing the boundary between acanthite and native silver, and silver solubility contours calculated using the data of (Gammons and Barnes 1989)

which do not apply at Shasta)

In contrast to gold, silver forms stable complexes with both bisulphide and chloride ligands under epithermal conditions (Seward, 1976, Gammons and Barnes, 1989). However, at the pH, a_{H_2S} and a_{Cl} interpreted for Shasta, the bisulphide complex should dominate (cf Gammons and Barnes, 1989).

In view of the above discussion, and the intimate paragenetic association of gold and silver (which suggests that they were similarly transported and deposited), we conclude that both metals were transported as bisulphide complexes and, accordingly, show contours of their solubility in this form on Figs 18 and 19. From these diagrams, it is evident that the evolution of the fluid to higher fO_2 and pH, documented above (and shown by the arrows), corresponds to sharp decreases in the solubility of both gold and silver. It is thus possible that deposition of these metals was caused by the increase in fO_2 and pH, which, as mentioned earlier, are predicted consequences of boiling. Other possible causes of Au-Ag deposition are the direct destabilization of bisulphide complexes as a result of the loss of H_2S to the vapour phase, or decreases in temperature, due to adiabatic expansion of the fluid.

In all probability, all of the above parameters played a role in Au-Ag deposition, as illustrated by the calculations of Seward (1989). These calculations show that just 4% of open system boiling of a saturated ore fluid at 290°C would result in the loss of 87% of the H_2 , 66% of the CO_2 , and 51% of the H_2S , leading to an increase in pH of two log units, significant increases in fO_2 ,

and a drop in temperature of 20°C (Seward, 1989). Virtually any combination of these changes in H₂S, pH, fO₂ or temperature would have been sufficient to have deposited almost all the gold and silver in the solution.

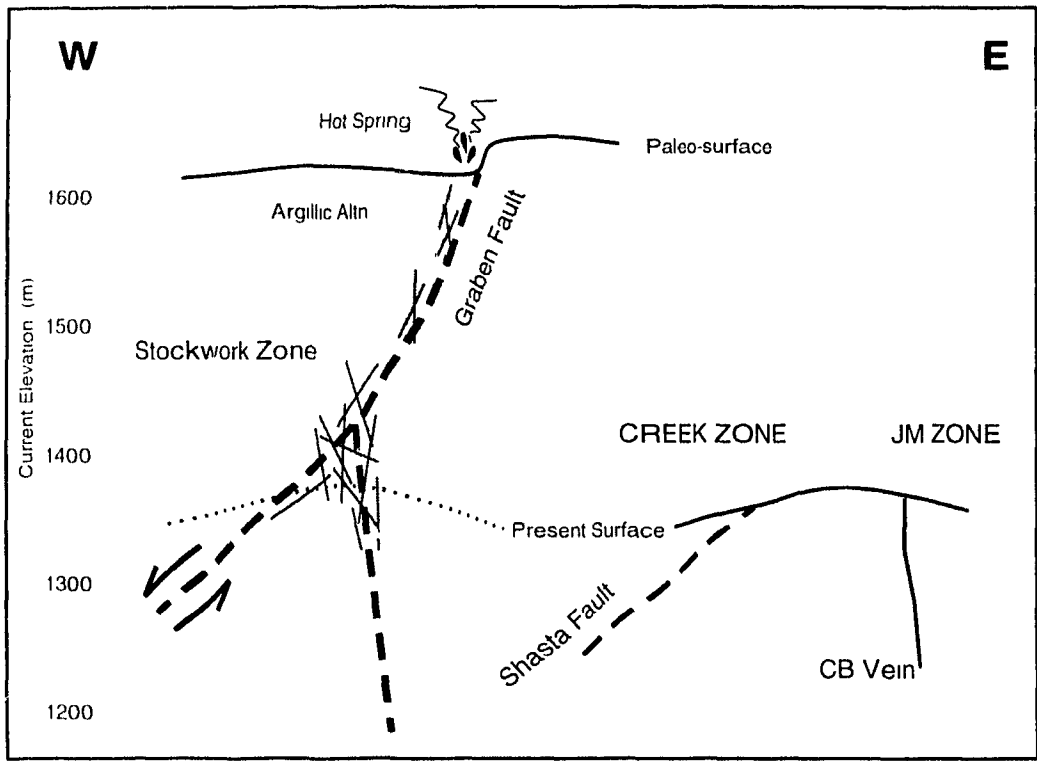
Deposit Model

The model which we favor is one in which hydrothermal fluids of meteoric origin were focused by faults and fracture zones, and mineral deposition occurred in response to boiling within these zones (Fig. 21). The discontinuous nature of the hydrothermal breccias at Shasta suggests that boiling may have been restricted, localized by rolls or constrictions in the fault plane, where throttling of the hydrothermal fluid could have occurred, and multi-stage breccias imply an episodic boiling history throughout the entire deposit.

According to this model, meteoric fluids were heated at depth by a cooling late-Toodoggone equivalent intrusion (such as the Black Lake stock or a similar body), and were circulated through the volcanic pile, leaching sulphur and metals (Fe, Cu, Pb, Zn, Au and Ag) mainly from enclosing volcanic rocks, thereby becoming enriched in Ca and C from interaction with propylitically altered country rock and/or underlying Asitka or Stuhini Group limestones. The fluid was then channelled along north-west trending normal faults and fracture zones towards the surface.

Initial boiling caused a rapid drop in temperature due to adiabatic expansion of the fluid, which resulted in quartz supersaturation and precipitation.

Figure 21 Conceptual model of the Shasta deposit



of early, fine-grained pre ore quartz and pyrite. Loss of volatile species to the vapour phase increased the pH of the fluid, thereby promoting potassic alteration by the liquid, and local sericitic alteration by the acidic vapours.

Quartz deposition caused partial or complete sealing of the hydrothermal conduit in many places, leading to throttling or overpressuring, respectively, at those locations. Where lithostatic pressure was exceeded, hydrofracturing occurred, resulting in explosive, decompressional fluid boiling which was responsible for ore stage mineralization. At this stage, calcite, sphalerite, chalcopyrite, galena and acanthite (\pm chlorite) became saturated and were precipitated, mainly as a result of an increase in pH. Electrum and native silver were then precipitated, in response to increased pH and/or oxygen fugacity and the decline in total sulphur concentration.

Finally, the fluid evolved to a point where the bulk of dissolved silica, base metals, silver and gold had been precipitated, and continued gentle boiling resulted in post-ore calcite (\pm hematite) deposition, during the waning stages of the hydrothermal system.

Comparison with Other Low Sulphidation Deposits

The Shasta deposit is similar to many low sulphidation deposits in the North American Cordillera in its spatial and (indirect) genetic association with intermediate-felsic volcanism, and structural localization by extensional faults. However, like other deposits in the Toodoggone River area of British Columbia,

Shasta is Jurassic in age, which is significantly older than similar deposits in the Basin and Range province of the Western United States where many of the deposits are Tertiary in age (Buchanan, 1981)

Mineralogically, Shasta shares many characteristics with the adularia-sericite class of epithermal deposits proposed by Hayba et al (1985) and Heald et al (1987), but it is atypical in its lack of vein adularia, and may be unique in that ore grade mineralization is so closely associated with calcite gangue (cf Buchanan, 1981, Berger and Eimon, 1982) Calcite is not uncommon in adularia-sericite epithermal deposits, but it is invariably late; ore mineralization is characteristically hosted by chalcedony, quartz or amethystine quartz, and adularia

The lack of vein adularia is somewhat unusual, but K-feldspar is abundant in proximal, potassically altered wall-rocks. This suggests that the wall-rocks may have been particularly reactive, perhaps due to their generally unwelded (i.e. porous) texture and/or relatively high-K chemistry (Diakow et al., 1991). Alternatively, the lack of vein adularia may simply reflect the level of exposure of the deposit, wherein characteristic "boiling textures" such as banded adularia and/or bladed quartz (replacing calcite), which may have occurred at higher levels in the system, have been eroded since the deposit was formed.

At the Lawyers deposit, "acanthite projects inward from the wall of [quartz] vugs with calcite in the interstices" (Vulimuri et al., 1986). This feature appears to reflect a paragenesis similar to that of the Shasta deposit, but chalcedony and

quartz are, nevertheless, the main ore hosts at Lawyers. The exclusive association between high grade silver-gold mineralization and the onset of calcite deposition in a boiling system, is apparently unique to the Shasta deposit, in the Toodoggone area.

SUMMARY AND CONCLUSIONS

The Shasta deposit is an example of volcanic-hosted precious metal mineralization which formed as a result of boiling in an epithermal environment. Its genesis began with the leaching of metals and sulphur from the Toodoggone volcanic pile by a meteoric fluid, which was heated at depth by a cooling subvolcanic intrusive. During circulation through the pile, the fluid became strongly enriched in $\delta^{18}\text{O}$ due to extensive wall rock interaction and low water/rock ratios. The fluid was relatively dilute, containing an average of 1-2 wt% NaCl eq, with approximate molal concentrations of 0.26 *m* NaCl, 0.1 *m* KCl, 0.04 *m* CaCl₂, and 0.01 *m* S.

After rising to a depth of about 750 m, boiling of the fluid caused hydrofracturing, deposition of pre-ore quartz (+pyrite) associated with potassic alteration, and local sealing of the conduit. Episodic boiling in response to alternating silica sealing, and throttling and/or hydro-brecciation, was responsible for ore deposition between 280 and 225°C. Ore minerals were precipitated concomitantly with the onset of calcite precipitation, and consisted of sphalerite, chalcopyrite, galena, acanthite, electrum and native silver. Local sericitic

alteration was caused by acidic vapours which separated during boiling. Post-ore calcite was precipitated during the waning stages of the hydrothermal system.

The initial conditions of the ore fluid were between $\log fO_2$ -31 to -33, and pH 4.25 to 6, but during ore deposition, the fluid evolved to more alkaline and oxidized conditions. Quartz and calcite were deposited in response to decreases in temperature and increases in pH, respectively. The increased pH also caused precipitation of base metal sulphides. Silver and gold were transported mainly as bisulphide complexes, and were deposited due to a loss of H_2S , and increases in oxygen fugacity and pH.

The Shasta deposit shares many characteristics of the low sulphidation, adularia-sericite class of epithermal deposit, but is unusual in its lack of vein adularia, bladed quartz (replacing calcite) and the typical epithermal trace elements of mercury, antimony and arsenic. Shasta may be unique in that high grade ore deposition was directly related to the onset of calcite precipitation in a boiling system, and may therefore represent a distinct "calcite transitional" subclass of low sulphidation or adularia-sericite epithermal deposit.

CHAPTER 3 CONCLUSIONS

- 1 Shasta is a volcanic-hosted epithermal silver-gold deposit of Jurassic age
Emplacement of the deposit was structurally controlled by fracture zones associated with graben faulting, but the occurrence of fine-grained quartz, abundant vapour-rich inclusions and the hydrothermal nature of ore grade breccias, indicate that ore deposition was controlled by boiling of the hydrothermal fluid
- 2 The hydrothermal fluid was of meteoric origin but became strongly enriched in $\delta^{18}\text{O}$ due extensive wall-rock interaction and low water/rock ratios. Ore metals were leached from the Toadogone volcanic pile during heating of the fluid by subvolcanic intrusives. The fluid was relatively dilute, averaging 1-2 wt% NaCl equivalent, and contained average concentrations of 0.26 m Na, 0.1 m K, 0.04 m Ca, and 0.01 m S
- 3 The mineralization history began with pre-ore quartz, deposited in early stockwork veins, followed by ore stage quartz-calcite, precipitated in hydrothermal breccias and reopened veins, and ended with post-ore calcite, deposited in the latest veins. Hydrothermal breccias were the result of throttling or over-pressuring of the vein fluid, due to partial or complete sealing of the hydrothermal conduit by the deposition of early quartz
- 4 Potassic wall-rock alteration observed in stockwork zones was associated

with early quartz deposition and was therefore not directly related to ore formation. Sericitic wall-rock alteration, observed locally in close proximity to ore grade quartz-calcite breccias, is interpreted to have been the result of interaction with acidic vapours separated from the boiling fluid.

5. Ore deposition occurred between 280 and 225°C in response to boiling of the hydrothermal fluid at a maximum depth of 750 m. Initial fluid conditions were approximately $\log f_{O_2}$ -31 to -33, and pH 4.25 to 6.0, and during ore deposition, the fluid evolved to higher values, which lead to the precipitation of silver-gold ore minerals concomitantly with the onset of calcite saturation.
6. Silver and gold were transported as bisulphide complexes, and were precipitated as a result of increased pH and/or oxygen fugacity, and decreased concentration of total sulphur, due to loss of CO_2 , H_2S and H_2 to the vapour phase during boiling. Quartz and calcite were deposited as a result of a decrease in temperature (due to adiabatic expansion) and an increase in pH, respectively. The increase in pH was also the main control on base metal (Fe, Zn, Cu, and Pb) deposition.
7. Shasta represents a calcite-rich example of the low sulphidation, adularia-sericite category of epithermal deposits. It is somewhat unusual in its lack of vein adularia, and may be unique in that ore deposition was directly related to a transition from quartz to calcite precipitation in a boiling hydrothermal system.

8. The exploration significance of the proposed model hinges on several features identified in this study, including the boiling/brecciation control on silver-gold mineralization; the strong association of high grade ore with the onset of calcite precipitation, and the spatial association of sericitic alteration with boiling. Consequently, sericitic alteration may provide a useful guide to exploration for potentially mineralized calcite-rich hydrothermal breccias. Furthermore, according to the interpreted morphology (north-west plunging, inverted "V"), structural setting (graben fault) and substantial paleo-depth of the deposit (750 m), the best mineralization potential may lie down plunge in the down-dropped graben block, west of the Shasta fault.

REFERENCES

- Barnes, H L , 1979, Solubilities of ore minerals, *in* Barnes, H L. (ed),
Geochemistry of Hydrothermal Ore Deposits, Second Edition: John Wiley
and Sons, New York, p 236-277.
- Barr, D A , 1978, Chappelle gold-silver deposit, British Columbia: Canadian
Mining and Metallurgy Bulletin, v. 71, no 790, p 66-79
- Berger, B R , and Eimon, P L , 1983, Conceptual models of epithermal precious
metal deposits, *in* Shanks, W.C III (ed), Cameron Volume on
Unconventional Mineral Deposits: Society of Mining Engineers, p 191-
205
- Bodnar, R J , 1983, A method of calculating fluid inclusion volumes based on
vapor bubble diameters and P-V-T-X properties of inclusion fluids.
Economic Geology, v 78, p 535-542.
- Buchanan, I J , 1979, The Las Torres mine, Guanajuato, Mexico: Ore controls
of a fossil geothermal system unpublished Ph D thesis, Colorado School
of Mines, 138 p
- Buchanan, L J , 1981, Precious metal deposits associated with volcanic
environments in the southwest, *in* Dickinson, W R., and Payne, W D.,
(eds), Relations of Tectonics to Ore Deposits in the South Cordillera:
Arizona Geological Society Digest, v 14, p. 237-261
- Carter, N C , 1972, Toodoggone River area *in* Geology, Exploration and Mining
in British Columbia, 1971 B.C. Ministry of Energy, Mines and Petroleum
Resources, p 63-71
- Cas, R A F , and Wright, J V., 1988, Volcanic Successions, Modern and Ancient:
London, Unwin Hyman Ltd , 487 p.
- Cathelineau, M , 1988. Cation site occupancy in chlorites and illites as a function
of temperature Clay Minerals, v. 23, p. 471-485.
- Clark, J R , and Williams-Jones, A E , 1987, Metallogenic implications of
lithotectonic assemblages in the Toodoggone Au/Ag district, north-central
British Columbia Geological Association of Canada, Program with
Abstracts, v 12, p 32.
- Clark, J R., and Williams-Jones, A E., 1988, A preliminary appraisal of the Au-Ag
metallogeny of the Toodoggone district, north-central British Columbia, *in*

Geology and Metallogeny of North-western British Columbia Workshop
Smithers Exploration Group - Geological Association of Canada, Program
with Abstracts, p A33-A37

- Clark, J R , and Williams-Jones, A E , 1989, New K Ar isotopic ages of
epithermal alteration from the Toodoggone River area, British Columbia
(94E) B.C Ministry of Energy, Mines and Petroleum Resources,
Geological Fieldwork 1988, Paper 1989-1, p 409-412
- Clark, J.R., and Williams-Jones, A E , 1990, $^{40}\text{Ar}/^{39}\text{Ar}$ ages of epithermal
alteration and volcanic rocks in the Toodoggone Au-Ag district, north-
central British Columbia (94) B C Ministry of Energy, Mines and
Petroleum Resources, Geological Fieldwork 1990, Paper 1991-1, p 207-
216.
- Clark, J.R., and Williams-Jones, A.E., 1990, Analogues of epithermal gold-silver
deposition in geothermal well scales Nature, v 346, no 6285, p 644-
645
- Cox, K G., Bell, J D , and Pankhurst, R J , 1979, The Interpretation of
Igneous Rocks London, George Allen and Unwin Ltd , 450 p
- Craig, H., 1961, Isotopic variations in meteoric waters, Science, v 133, p 1702-
1703.
- de Ronde, C.E J., and Blattner, P , 1988, Hydrothermal alteration, stable
isotopes and fluid inclusions of the Golden Cross epithermal gold-silver
deposit, Waihi, New Zealand. Economic Geology, v 83, p 895-917
- Diakow, L.J , 1984, Geology between Toodoggone and Chukachida Rivers
(94E) B.C. Ministry of Energy, Mines and Petroleum Resources,
Geological Fieldwork 1983, Paper 1984-1, p 139-145
- Diakow, L.J., Panteleyev, A , and Schroeter, T G , 1985, Geology of the
Toodoggone River area (94E). B C Ministry of Energy, Mines and
Petroleum Resources, Preliminary Map 61
- Daikow, L.J., 1990, Volcanism and evolution of the Early and Middle Jurassic
Toodoggone Formation, Toodoggone mining distict, British Columbia
unpublished Ph.D thesis, University of Western Ontario, 180 p
- Diakow, L.J., Panteleyev, A , and Schroeter, T.G , 1991, Jurassic epithermal
deposits in the Toodoggone River area, northern British Columbia
Examples of well-preserved, volcanic hosted, precious metal

mineralization. *Economic Geology*, v. 86, p. 529-554

- Drummond, S E , and Ohmoto, H , 1985, Chemical evolution and mineral deposition in boiling hydrothermal systems. *Economic Geology*, v 80, p. 126-147
- Field, C W , and Fifarek, R H., 1985, Light stable isotope systematics in the epithermal environment, *in* Berger, B.R , and Bethke, P M , (eds), *Geology and Geochemistry of Epithermal Systems: Society of Economic Geologists, Reviews in Economic Geology*, v 2, p 99-128
- Forster, D G , 1984, Geology, petrology and precious metal mineralization, Toodoggone River area, north-central British Columbia; unpublished M.Sc. thesis, University of British Columbia, 167 p
- Friedman, I , and O'Neil, J R , 1977, Compilation of stable isotope fractionation factors of geochemical interest, *in* Fleisher, M , (ed.), *Data of Geochemistry, Sixth Edition: U S Geological Survey, Professional Paper 440-KK*, p KK1-KK12
- Gabrielse, H , Dodds, C J , and Mansy, J L., 1976, Toodoggone River (94E) map area. Geological Survey of Canada, Open File 306.
- Gammons, C H., and Barnes, H L., 1988, The solubility of Ag_2S in near neutral aqueous sulphide solutions at 25 to 300°C. *Geochimica et Cosmochimica Acta*, v 53, p 279-290
- Haas, J L , Jr , 1971, The effect of salinity on the maximum thermal gradients of a hydrothermal system at hydrostatic pressure. *Economic Geology*, v. 66, p. 940-946.
- Hayashi, K , and Ohmoto, H , 1988, Solubility of gold in NaCl- and H_2S -bearing aqueous solutions at 250-350°C: *Geochimica et Cosmochimica Acta*, v. 55, p. 2111-2126.
- Hayba, D O , Bethke, P M , Heald, P., and Foley, N.K , 1985, Geologic, mineralogic and geochemical characteristics of volcanic hosted epithermal precious-metal deposits, *in* Berger, B R , and Bethke, P M., (eds.), *Geology and Geochemistry of Epithermal Systems: Society of Economic Geologists, Reviews in Economic Geology*, v. 2, p. 129-167.
- Haynes, F M , Sterner, S M and Bodnar, R J., 1988, Synthetic fluid inclusions in natural quartz, IV. Chemical analyses of fluid inclusions by SEM/EDA: Evaluation of method. *Geochimica et Cosmochimica Acta*, v. 52, p. 969-

- Heald, P., Foley, N.K, and Hayba, D O , 1987, Comparative anatomy of volcanic-hosted epithermal deposits acid-sulphate and adularia-sericite types Economic Geology, v 82, p 1-26
- Hedenquist, J W , 1987, Mineralization associated with volcanic-related hydrothermal systems in the Circum-Pacific Basin, *in* Circum-Pacific Energy Mineral Resources Conference, 4th, Singapore, p 513-524
- Henley, R.W., 1985, Geothermal framework for epithermal ore deposits, *in* Berger, B R., and Bethke, P M , (eds), Geology and Geochemistry of Epithermal Systems: Society of Economic Geologists, Reviews in Economic Geology, v 2, p 1-24
- Henley, R W , and Ellis, A J , 1983, Geothermal systems, ancient and modern - A geochemical review Earth Science Reviews, v 19, p 1-50
- Johnson, J W , Oelkers, E H , and Helgeson, H C , 1991, A software package for calculating the standard molal thermodynamic properties of minerals, gases, aqueous species, and reactions from 1 to 5000 bars and 0° to 1000°C: Laboratory of Theoretical Geochemistry, University of California, Berkley, 101 p
- Kamilli, R.J , and Ohmoto, H , 1977, Paragenesis, zoning, fluid inclusion and isotopic studies of the Finlayson Vein, Colque District, central Peru Economic Geology, v. 72, p 950-982
- Kwak, T.A P , 1990, Geochemical and temperature controls on ore mineralization at the Emperor Gold Mine, Vatukoula, Fiji, *in* Hedenquist, J.W., White, N C , and Siddeley, G , (eds), Epithermal Gold Mineralization of the Circum-Pacific: Geology, Geochemistry, Origin and Exploration, II Journal of Geochemical Exploration, v 36, p 297-337
- Lindgren, W., 1933, Mineral deposits McGraw-Hill Book Company, New York, 930p.
- Marsden, H , and Moore, J.M , 1989, Stratigraphy and structural setting of the Shasta silver-gold deposit, north-central British Columbia B C Ministry of Energy, Mines and Petroleum Resources, Geological Fieldwork 1988, Paper 1989-1, p 395-407.
- Marsden, H , and Moore, J M , 1990, Stratigraphy and structural setting of the Shasta silver-gold deposit B C Ministry of Energy, Mines and Petroleum

Resources, Geological Fieldwork 1989, Paper 1990-1, p. 305-314.

- Marsden, H , 1990, Stratigraphy, structure and tectonic setting of the Shasta silver-gold deposit, north-central British Columbia, unpublished M Sc thesis, Carlton University, 213p
- Matsuhisa, Y , Goldsmith, J R , and Clayton, R N , 1979, Oxygen isotopic fractionation in the system quartz-albite-anorthite-water *Geochimica et Cosmochimica Acta*, v 43, p. 1131-1140.
- McPherson, M D , Oye, H , and Holbek, P M , 1991, 1990 exploration report on the Shasta claim group, unpublished company report, Homestake Canada Ltd , 70 p
- Ohmoto, H., 1972, Systematics of sulphur and carbon isotopes in hydrothermal ore deposits: *Economic Geology*, v 67, p 551-578
- Ohmoto, H , and Rye, R O , 1974, Hydrogen and oxygen isotopic compositions of fluid inclusions in the Kuroko deposits, Japan *Economic Geology*, v 69, p 947-953
- Ohmoto, H , and Rye, R O , 1979, Isotopes of sulphur and carbon, *in* Barnes, H L (ed), *Geochemistry of Hydrothermal Ore Deposits*, Second Edition John Wiley and Sons, New York, p 509-567.
- O'Neil, J R , and Taylor, H P., 1967, The oxygen isotope and cation exchange chemistry of feldspars *American Mineralogist*, v 52, p 1414-1437.
- Oakes, C S , Bodnar, J D , and Simonson, J M. 1990, The system NaCl-CaCl₂-H₂O, I The ice liquidus at 1 atm total pressure *Geochimica et Cosmochimica Acta*, v 54, p 603-610
- Panteleyev, A , 1982, Toodoggone volcanics south of the Finlay River (94E/2) B.C. Ministry of Energy, Mines and Petroleum Resources, Geological Fieldwork 1981, Paper 1982-1, p. 135-141.
- Panteleyev, A , 1983, Geology between Toodoggone and Sturdee Rivers. B.C. Ministry of Energy, Mines and Petroleum Resources, Geological Fieldwork 1982, Paper 1983-1, p 143-148.
- Phillips, G N , and Groves, D.I., 1984, An epigenetic origin for Archean banded iron-formation-hosted gold deposits *Economic Geology*, v 79, p. 162-171.
- Potter, R.W , Clyne, M A , and Brown, D L , 1978, Freezing point depression

of aqueous sodium chloride solutions: *Economic Geology*, v 73, p 284-285.

Reed, M H , and Spycher, N F , 1985, Boiling, cooling and oxidation in epithermal systems a numerical modeling approach, *in* Berger, B R , and Bethke, P M , (eds), *Geology and Geochemistry of Epithermal Systems* Society of Economic Geologists, *Reviews in Economic Geology*, v 2, p 249-272

Romberger, S B , 1990, Transport and deposition of precious metals in epithermal deposits, *in* Cuffney, B , (ed), *Geology and Ore Deposits of the Great Basin* Geological Society of Nevada, p 219-231

Sander, M V , and Einaudi, M.T , 1990, Epithermal deposition of gold during transition from propylitic to potassic alteration at Round Mountain, Nevada *Economic Geology*, v 85, p 285-311

Shenburger, D.M , and Barnes, H L., 1988, Solubility of gold in aqueous sulphide solutions from 150 to 350°C *Geochimica et Cosmochimica Acta*, v 53, p 269-278

Schroeter, T G , 1982, Toadoggone River area (94E) B C Ministry of Energy, Mines and Petroleum Resources, *Geological Fieldwork 1981*, Paper 1982-1, p. 122-133

Schroeter, T G , Diakow, L J , and Panteleyev, A , 1986, Toadoggone River area (94E). B C Ministry of Energy, Mines and Petroleum Resources, *Geological Fieldwork 1985*, Paper 1986-1, p 167-168

Scott, S D , and Barnes, H L , 1971, Sphalerite geothermometry and geobarometry. *Economic Geology*, v 66, p 653-669

Seward, T M , 1973, Thio complexes of gold and the transport of gold in hydrothermal ore solutions, *Geochimica et Cosmochimica Acta*, v 37, p 370-399.

Seward, T M , 1976, The stability of chloride complexes of silver in hydrothermal solutions up to 350°C *Geochimica et Cosmochimica Acta*, v 40, p 1329-1341.

Seward, T M., 1989, The hydrothermal chemistry of gold and its implications for ore formation: boiling and conductive cooling as examples *Economic Geology*, Monograph 6, p. 398-404

- Silberman, M L , and Berger, B R , 1985, Relationship of trace-element patterns to alteration and morphology in epithermal precious metal deposits, in Berger, B R , and Bethke, P M , (eds), *Geology and Geochemistry of Epithermal Systems* Society of Economic Geologists, *Reviews in Economic Geology*, v 2, p 203-232
- Taylor, H P , Jr , 1979, Oxygen and hydrogen isotope relationships in hydrothermal mineral deposits, *in* Barnes, H.L (ed), *Geochemistry of Hydrothermal Ore Deposits*, Second Edition. John Wiley and Sons, New York, p 236-277
- Tipper, H W , and Richards, T A , 1976, Jurassic stratigraphy and history of north-central British Columbia: Geological Survey of Canada, Bull. 270, 73 p
- Werre, R W , Jr , Bodnar, R J., Bethke, P M., and Barton, P B., Jr., 1979, A novel gas-flow fluid inclusion heating/freezing stage, (abstr.). *Geological Society of America Program Abstracts*, v 11, 539 p
- White, D E , 1974, Diverse origins of hydrothermal ore fluids *Economic Geology*, v 69, p 954-973
- White, D E , 1981, Active geothermal systems and hydrothermal ore deposits: *Economic Geology*, 75th Anniversary Volume, p. 392-423.
- Vulimiri, V R , Tegart, P , and Stammers, M.A , 1986, Lawyers gold-silver deposits, *in* Morin, J.A. (ed), *Mineral Deposits of Northern Cordillera: Canadian Institute of Mining and Metallurgy, Special Volume 37*, p. 191-201

APPENDIX I

Whole-rock Geochemical, Silver and Gold Assay Data for DDH90-09 and DDH90-10.

Sample	From	Ag	Au	Cu	Pb	Zn	SiO ₂	Al ₂ O ₃	Fe ₂ O ₃	MgO	CaO	Na ₂ O	K ₂ O	TiO ₂	P ₂ O ₅	MnO	Cr ₂ O ₃
90901	5.1	2.2	0.79	9	58	96	69.73	11.14	2.68	0.70	4.14	1.73	5.48	0.29	0.10	0.20	0.024
90902	6.1	39.4	1.22	19	54	102	64.01	11.64	2.85	0.87	6.39	1.77	5.35	0.30	0.11	0.29	0.02
90903	18.1	54.2	2.28	13	11	38	77.00	9.77	1.70	0.66	2.31	1.38	4.91	0.24	0.07	0.17	0.074
90904	19.6	30.2	1.88	7	40	66	77.52	9.60	1.88	0.80	2.21	1.21	5.14	0.26	0.09	0.14	0.037
90905	20.6	79.6	3.33	38	548	596	58.14	4.10	1.93	0.92	18.80	0.07	2.21	0.11	0.09	0.46	0.026
90906	21.5	326.0	3.89	61	717	716	67.84	6.35	2.40	0.69	11.21	0.22	3.80	0.16	0.05	0.27	0.023
90907	22.4	231.0	3.37	35	259	184	64.78	9.71	3.15	0.65	9.49	0.62	5.59	0.24	0.11	0.28	0.016
90908	23.4	158.0	1.63	23	144	124	56.85	10.41	3.18	0.81	13.13	0.92	6.19	0.26	0.11	0.39	0.016
90909	24.4	1070.0	10.95	63	514	714	57.04	10.36	3.12	0.39	13.29	1.12	4.92	0.28	0.13	0.43	0.015
90910	25.4	470.0	7.32	43	381	634	51.03	7.91	2.46	1.22	19.10	0.82	3.67	0.21	0.10	0.54	0.019
90911	26.4	1240.0	17.98	80	649	1101	43.67	6.66	2.82	1.12	24.21	0.37	4.21	0.15	0.11	0.62	0.017
90912	27.4	472.0	6.50	22	131	209	73.69	11.27	1.67	0.58	2.60	0.40	7.89	0.25	0.05	0.12	0.043
90913	28.7	68.0	0.85	15	84	103	71.08	11.96	2.83	0.98	3.20	1.43	5.91	0.30	0.11	0.22	0.023
90914	30.1	150.0	2.66	19	76	113	57.94	10.97	2.50	0.90	12.61	1.10	3.96	0.26	0.08	0.36	0.02
90915	31.6	164.0	1.68	22	132	133	61.06	9.52	2.92	0.79	12.44	0.89	3.64	0.24	0.10	0.35	0.025
90916	33.1	132.0	1.39	23	92	172	66.42	13.55	3.41	1.28	4.90	1.79	4.04	0.32	0.19	0.21	0.021
90917	34.1	151.0	1.60	18	74	146	65.46	13.70	3.67	1.12	5.45	1.80	3.80	0.34	0.12	0.19	0.021
90918	35.2	30.0	0.30	15	22	62	63.91	13.04	3.21	1.06	6.88	1.95	3.80	0.32	0.09	0.23	0.019
90919	36.7	80.2	0.95	11	56	95	68.96	11.89	2.93	1.05	5.14	1.83	4.07	0.30	0.09	0.21	0.021
90920	38.2	79.4	1.19	27	71	93	66.18	10.41	2.58	0.88	8.34	1.49	4.04	0.25	0.06	0.24	0.023

APPENDIX I (cont)

Sample	From	Ag	Au	Cu	Pb	Zn	SiO ₂	Al ₂ O ₃	Fe ₂ O ₃	MgO	CaO	Na ₂ O	K ₂ O	TiO ₂	P ₂ O ₅	MnO	Cr ₂ O ₃
91001	4.0	28.0	0.36	17	29	57	67.55	9.02	2.37	0.63	8.65	1.31	4.34	0.24	0.06	0.25	0.029
91002	5.5	12.5	0.43	11	15	71	69.44	12.54	3.26	1.07	3.59	2.36	4.98	0.32	0.11	0.19	0.019
91003	7.0	20.1	0.57	10	25	59	68.58	12.50	3.23	1.06	3.80	2.24	5.29	0.33	0.09	0.23	0.02
91004	8.5	22.6	0.46	11	630	259	69.71	13.10	3.32	1.05	2.54	2.41	5.39	0.34	0.14	0.21	0.019
91005	10.0	9.4	0.22	12	57	106	68.50	13.74	3.42	1.43	2.46	2.79	5.12	0.36	0.14	0.26	0.017
91006	11.5	258.0	3.20	35	351	645	69.06	12.59	3.68	1.85	2.69	2.20	4.80	0.32	0.11	0.36	0.019
91007	13.0	24.2	0.45	15	59	111	70.20	12.99	3.45	1.18	2.20	2.38	5.33	0.33	0.12	0.21	0.023
91008	14.5	34.2	0.66	14	71	126	69.13	11.61	3.02	1.10	4.70	1.95	4.77	0.29	0.09	0.28	0.025
91009 *	16.0	6.0	0.15	13	21	101	67.88	14.13	3.62	1.40	2.90	2.46	4.67	0.37	0.14	0.23	0.018
91010	18.1	274.0	3.59	27	325	302	61.68	11.08	3.67	1.64	8.85	1.71	4.61	0.27	0.09	0.41	0.018
91011	18.9	352.0	6.49	27	388	367	52.73	9.03	3.35	1.38	15.92	1.26	3.92	0.22	0.09	0.52	0.018
91012	19.9	81.5	1.30	19	134	155	70.16	12.57	3.41	1.13	2.35	2.08	5.37	0.32	0.12	0.27	0.021
91013	20.5	730.0	11.50	53	38	124	62.15	9.95	3.63	2.03	9.14	1.29	3.76	0.23	0.08	0.52	0.024
91014	21.0	386.0	6.53	3.	683	892	64.58	8.86	2.82	1.24	9.71	1.17	3.59	0.22	0.11	0.39	0.025
91015	22.0	387.0	7.89	27	745	910	63.99	8.70	2.91	1.12	10.00	0.96	4.07	0.22	0.04	0.37	0.023
91016	23.1	620.0	7.55	37	1218	2537	47.84	2.16	1.09	0.46	26.78	0.10	1.30	0.05	0.06	0.63	0.02
91017	23.6	580.0	7.11	32	403	603	63.70	5.66	1.85	0.64	13.41	0.48	3.31	0.12	0.06	0.30	0.02
91018	24.3	230.0	2.01	13	149	243	60.15	7.70	2.13	0.55	13.49	0.47	4.80	0.18	0.12	0.37	0.023
91019	25.3	23.0	0.41	4	20	60	59.76	10.72	2.88	0.95	10.47	0.91	4.87	0.27	0.16	0.38	0.016
91020	26.3	14.3	0.19	5	17	80	67.41	13.04	3.14	1.22	3.81	1.86	4.70	0.33	0.14	0.25	0.018
91021	27.5	64.4	0.62	8	59	118	61.66	10.19	2.92	1.35	9.65	1.51	3.74	0.27	0.14	0.38	0.019
91022	29.0	28.3	0.25	6	31	122	62.87	12.85	3.29	1.47	6.70	1.89	3.81	0.33	0.16	0.31	0.017
91023	30.7	47.2	0.56	11	62	143	67.26	12.63	3.07	1.26	4.39	1.68	4.54	0.32	0.10	0.27	0.021
91024	32.7	96.0	0.81	12	92	183	65.16	9.44	2.63	1.32	8.49	1.21	3.77	0.23	0.10	0.37	0.028
91025	34.0	30.2	0.41	6	14	69	61.98	10.22	2.59	1.06	9.83	1.44	4.51	0.24	0.12	0.37	0.021
91026	35.5	4.4	0.12	10	10	64	63.65	13.16	3.10	1.19	5.90	1.69	5.05	0.32	0.22	0.28	0.022

* Least altered reference sample used for mass balance calculations

APPENDIX II

Fluid Inclusion Data

Sample	Mineral	T _n °C	T _e °C	T _m ice °C	Salinity*
87-23-38 7	CAL	283 8	-	-0 1	0 2
87-23-38 7	CAL	245 8	-	-0 5	0 9
87-23-38 7	CAL	264 3	-	-1 3	2 4
87-23-38 7	CAL	278 2	-	-	-
87-23-38 7	CAL	267 5	-	0 0	0 0
87-23-38 7	CAL	283 0	-	-	-
87-23-38 7	CAL	303 0	-	0 0	0 0
87-23-38 7	CAL	284 9	-	-0 3	0 5
87-23-38 7	QTZ	300 0	-	-0 2	0 4
87-23-38 7	QTZ	247 0	-	-0 3	0 5
87-23-38 7	QTZ	267 2	-	-0 2	0 4
87-23-38 7	QTZ	225 0	-	-0 3	0 5
87-23-38 7	MINCAL	197 0	-	-	-
87-23-38 7	MINCAL	263 0	-	-	-
87-23-38 7	MINCAL	285 0	-	-	-
87-23-38 7	MINCAL	287 0	-	-	-
87-23-38 7	CAL	238 0	-	-2 0	3 7
87-23-38 7	CAL	235 0	-	-1 3	2 4
87-23-38 7	CAL	269 5	-1 0	0 6	1 1
87-23-38 7	CAL	245 0	-	-	-
87-23-38 7	CAL	291 0	-	-	-
87-23-38 7	CAL	274 8	-0 8	-0 4	0 7
87-23-38 7	QTZ	307 3	-1 7	-1 2	2 2
87-23-38 7	CAL	139 0	-1 8	-0 3	0 5
87-23-38 7	CAL	204 0	-	-	-
87-23-38 7	CAL	254 7	-0 3	0 0	0 0
87-23-38 7	CAL	225 0	-0 3	0 0	0 0
87-23-38 7	CAL	250 0	-	-	-
87-23-38 7	CAL	-	-1 3	-0 6	1 1
87-23-38 7	MIN QTZ	224 0	-	-	-
87-23-38 7	MIN QTZ	264 4	-	-	-
87-23-38 7	MIN QTZ	295 5	-0 7	-0 2	0 4
89-04-35 6	MIN QTZ	275 5	-0 8	-0 2	0 4
89-04-35 6	MIN QTZ	275 2	-0 9	-0 2	0 4
89-04-35 6	MIN QTZ	296 8	-	-1 4	2 6
89-04-35 6	MIN QTZ	305 9	-	-0 6	1 1
89-04-35 6	QTZ	280 5	-2 2	-1 7	3 1
89-04-35 6	MIN QTZ	163 2	-	-	-
89-04-35 6	MIN QTZ	185 2	-	-	-
89-04-35 6	MIN QTZ	225 9	-	-	-
89-04-35 6	MIN QTZ	269 5	-	-	-
89-04-35 6	MIN QTZ	158 6	-0 5	0 0	0 0

Sample	Mineral	T _n °C	T _p °C	T _m ice °C	Salinity*
89-04-35 6	MIN QTZ	261 0	-0 6	-0 2	0 4
89-04-35 6	MIN QTZ	303 0	-0 5	0 0	0 0
89-04-35 6	MIN QTZ	252 0	-0 4	0 0	0 0
89-04-35 6	MIN QTZ	253 0	-0 4	0 0	0 0
89-04-35 6	MIN QTZ	262 0	-	-	-
89-04-35 6	MIN QTZ	300 0	-0 5	-0 1	0 2
89-04-35 6	MIN QTZ	193 5	-0 1	0 5	0 9
89-04-35 6	MIN QTZ	264 5	-	0 2	0 4
89-04-35 6	MIN QTZ	287 4	-0 1	0 0	0 0
89-04-35 6	MIN QTZ	292 7	-0 4	0 1	0 2
89-04-35 6	MIN QTZ	300 7	-	-	-
89-04-35 6	MIN QTZ	222 9	-	-	-
89-04-35 6	MIN QTZ	218 3	-	-	-
89-04-35 6	MIN QTZ	291 6	-	-	-
87-12-95 4	MIN CAL	263 8	-	-	-
87-12-95 4	MIN CAL	232 5	-2 4	-1 6	2 9
87-12-95 4	MIN CAL	252 4	-	-1 1	2 0
87-12-95 4	MIN CAL	265 6	-	-0 9	1 6
87-12-95 4	MIN CAL	284 9	-	-0 6	1 1
87-12-95 4	MIN CAL	284 6	-	-0 7	1 3
87-12-95 4	MIN CAL	281 5	-	-0 8	1 4
83-6-55 7	CAL	223 0	-2 0	-1 4	2 6
83-6-55 7	CAL	175 0	-2 2	0 4	0 7
83-6-55 7	CAL	277 0	-1 5	-0 4	0 7
89-28-76 4	CAL	280 0	-	-	-
88-01-116 5	CAL	265 0	-	-	-
88-01-116 5	CAL	260 0	-	-	-
88-01-116 5	CAL	277 0	-	-	-
88-01-116 5	CAL	287 2	-1 2	-0 6	1 1
88-01-116 5	CAL	284 3	-	-1 4	2 6
88-01-116 5	CAL	281 3	-	-	-
88-01-116 5	CAL	213 6	-	0 0	0 0
88-01-116 5	CAL	272 8	-0 9	-0 1	0 2
88-01-116 5	CAL	299 6	-2 0	-0 4	0 7
88-01-116 5	CAL	290 4	-2 5	-0 7	1 3
88-01-116 5	CAL	266 8	-	-	-
88-01-116 5	CAL	285 3	-3 0	-1 0	1 8
88-01-116 5	CAL	268 7	-4 0	-0 9	1 6
88-01-116 5	CAL	256 5	-2 0	0 0	0 0
88-01-116 5	CAL	283 1	-2 0	-0 6	1 1
88-01-116 5	CAL	260 4	-2 0	-0 1	0 2
88-01-116 5	CAL	265 7	-	-	-
88-01-116 5	CAL	261 9	-2 0	0 0	0 0
88-01-116 5	CAL	301 5	-3 0	-0 1	0 2
88-15-89 6	CAL	229 9	-	0 0	0 0
88-15-89 6	CAL	145 0	-	-	-
88-15-89 6	CAL	182 0	-	-	-
88-15-89 6	CAL	265 7	-0 8	0 0	0 0

Sample	Mineral	T _n °C	T _n °C	T _n ice °C	Salinity*
88-15-89 6	CAL	197 8	-	0 0	0 0
88-15-89 6	CAL	187 0	-	-	-
88-15-89 6	CAL	240 5	-	-	-
88-15-89 6	CAL	208 0	-	-	-
88-15-89 6	CAL	185 0	-	-	-
88-15-89 6	CAL	199 0	-	-0 1	0 2
88-15-89 6	CAL	229 5	-	-0 5	0 9
84-2-40 0	CAL	217 0	-3 0	-0 4	0 7
84-2-40 0	CAL	240 0	-	-	-
84-2-40 0	CAL	192 0	-	-	-
84-2-40 0	CAL	222 0	-4 0	-1 5	2 8
84-2-40 0	CAL	233 0	-	-1 5	2 8
84-2-40 0	CAL	226 0	-3 0	-1 5	2 8
84-2-40 0	CAL	236 0	-6 0	-1 2	2 2
84-2-40 0	CAL	230 0	-	-0 1	0 2
84-2-40 0	CAL	242 0	-	-0 1	0 2
84-2-40 0	CAL	241 0	-	-	-
84-2-40 0	CAL	230 0	-	-0 1	0 2
84-2-40 0	CAL	245 0	-2 0	0 0	0 0
84-2-40 0	CAL	256 0	-	-	-
84-2-40 0	CAL	255 0	-	-	-
84-2-40 0	CAL	240 0	-4 0	0 0	0 0
84-2-40 0	CAL	225 0	-4 0	0 0	0 0
84-2-40 0	CAL	193 0	-5 0	-1 3	2 4
84-2-40 0	CAL	200 0	-2 0	0 0	0 0
84-14-70 3	MIN QTZ	286 0	-9 0	-1 0	1 8
84-14-70 3	QTZ	210 5	-6 0	-1 5	2 8
84-14-70 3	CAL	219 0	-4 0	-1 8	3 3
84-14-70 3	CAL	225 0	-6 0	-1 5	2 8
84-14-70 3	CAL	223 0	-5 0	-1 5	2 8
84-14-70 3	CAL	205 0	-	-	-
84-14-70 3	CAL	228 0	-5 0	-1 3	2 4
84-14-70 3	CAL	225 0	-	-1 3	2 4
84-14-70 3	CAL	288 0	-	-	-
87-11-65 2	CAL	292 1	-1 1	-0 3	0 5
87-11-65 2	CAL	271 8	-1 2	-0 2	0 4
87-11-65 2	CAL	287 2	-	-0 3	0 5
87-11-65 2	CAL	273 3	-2 2	-0 3	0 5
87-11-65 2	CAL	273 2	-	-	-
87-11-65 2	CAL	279 5	-3 0	-0 7	1 3
87-11-65 2	CAL	276 4	-3 5	-0 8	1 4
87-11-65 2	CAL	271 4	-	-0 8	1 4
87-11-65 2	CAL	276 3	-	-	-
87-11-65 2	CAL	276 4	-	-	-
87-11-65 2	CAL	274 7	-	-0 8	1 4
87-11-65 2	CAL	284 7	-2 1	-0 6	1 1
87-11-65 2	CAL	271 2	-2 4	-0 6	1 1
87-11-65 2	CAL	297 7	-1 8	-0 6	1 1

Sample	Mineral	T _h °C	T _e °C	T _m ice °C	Salinity*
87-11-65 2	CAL	285 0	-2 8	-0 7	1 3
87-11-80 6	QTZ	290 5	-3 0	-0 8	1 4
87-11-80 6	QTZ	215 6	-5 0	-2 0	3 7
87-11-80 6	QTZ	288 5	-	-1 7	3 1
87-11-80 6	QTZ	306 0	-	-0 3	0 5
87-11-80 6	QTZ	289 0	-4 6	-1 9	3 5
87-11-80 6	QTZ	275 0	-	-1 6	2 9
87-11-80 6	CAL	256 0	-4 2	-0 2	0 4
87-11-80 6	CAL	285 2	-4 0	-2 0	3 7
87-11-80 6	CAL	288 1	-	-0 1	0 2
87-11-80 6	MINQTZ	279 8	-	-	-
87-11-80 6	MINQTZ	273 1	-5 0	-0 3	0 5
87-11-80 6	MINQTZ	289 8	-	0 0	0 0
87-11-80 6	MINQTZ	300 0	-5 0	-0 2	0 4
87-11-80 6	MINQTZ	286 5	-	-	-
87-11-80 6	MINQTZ	296 0	-3 0	0 0	0 0
87-11-80 6	MINQTZ	306 0	-4 6	-0 1	0 2
87-11-80 6	MINQTZ	300 0	-7 0	-1 4	2 6
87-11-80 6	MINQTZ	274 7	-7 0	-1 3	2 4
87-11-80 6	MINQTZ	250 4	-	-	-
87-11-80 6	MINQTZ	274 7	-4 0	-1 2	2 2
87-11-80 6	MINQTZ	259 6	-	-1 1	2 0
87-11-80 6	MINQTZ	253 7	-	-	-

* Salinity calculated using the equation on Oakes et al , (1990)

APPENDIX III
Microprobe Analyses

Table 1 Fluid Inclusion Decrepitate Data (wt%)

	Na	Ca	K	Cl	S
JM87-23	28.76	0.00	12.76	58.48	0.00
	30.69	0.00	0.00	69.31	0.00
	33.29	19.90	12.45	34.36	0.0
	29.67	13.18	8.78	35.57	12.81
	36.82	0.00	0.00	62.02	1.16
	19.48	1.56	26.15	51.58	1.23
	39.90	6.01	0.00	50.71	3.38
CK89-04	23.84	4.46	21.24	42.26	8.21
	22.74	9.44	13.59	41.66	12.56
	20.92	11.83	22.39	35.99	8.88
	12.20	18.12	20.89	41.08	7.71
	14.75	13.02	25.62	40.55	6.06
	14.10	18.70	23.08	37.05	7.07
JM 87-11	22.83	5.63	23.90	47.6	0.00
	20.86	8.03	15.90	46.4	8.88
	20.96	12.32	19.50	43.01	4.22
	26.67	9.16	16.30	44.02	3.84
	37.62	21.47	8.70	32.22	0.00
	22.92	6.22	28.05	38.66	4.15
<hr/>					
Average (wt%)	Na	Ca	K	Cl	S
	25.21	9.42	15.75	44.87	4.75
<hr/>					
Average (at%)	Na	Ca	K	Cl	S
	34.01	7.35	12.50	39.52	6.6
<hr/>					
Atomic Ratios	Na/Cl	Ca/Na	K/Na	All/Cl	S/Cl
	0.86	0.22	0.37	1.36	0.17
<hr/>					
Molal Concentration*	Na	Ca	K	S	
	0.26	0.06	0.1	0.01	

* Estimated assuming 2wt% Na eq = 0.4m

Table 2 Sulphur Isotope Data

Sample	Grade Au/Ag (g/t)	Measured $\delta^{34}\text{S}$ (‰)	Calculated ¹ $\delta^{34}\text{S}_{\text{H.S.}}$ (‰)	
			280°C	225°C
Pyrite Separates				
CREEK ¹	14.6 / 134.0	-3.4	-4.7	-5.0
JMTC5-3	0.6 / 55.5	-3.5	-4.8	-5.1
CRK-1 ¹	1.9 / 61.5	-3.8	-5.1	-5.4
JMHG-PT	71.1 / 7271.7	-4.7	-6.0	-6.3
JMPTHG-D1	345.0 / 22,100.0	-5.0	-6.3	-6.6
JMPTHG-D2	225.9 / 88,374.0	-5.6	-6.9	-7.2
JMHGTR-B	9.4 / 371.0	-5.7	-7.0	-7.3
Composites				
JMPT-CBV	1015.0 / 17,518.0 (70% ZnS, 24% PbS, 6% Ag ₂ S)	-5.4	-5.0	-4.9
JMPTHG-D2	225.9 / 88,374.0 (34% ZnS, 36% PbS, 30% Ag ₂ S)	-7.3	-5.9	-5.6
Bulk Country Rock:				
8-1 42 5	barren	-0.7		
8-31 25 7	02 / 1 0	-2.5		
8-31 25 7	duplicate	-2.5		

1 Quartz-hosted mineralization

2 Calculations based on the equations of Ohmoto and Rye (1979)

Table 3 Oxygen and Hydrogen Isotope Data

Sample	Measured $\delta^{18}\text{O}$ (‰)			Calculated ¹ $\delta^{18}\text{O}_{\text{fluid}}$ (‰)		
	Qtz	Cal	Chl	280°C		225°C
JMHGPT	6.4	3.6		-1.2	-2.6	-4.7
CBVEIN	6.0	3.9		-1.6	-2.3	-4.4
HGTR-B		4.0			-2.2	-4.3
84-14-72 3		5.7			-0.5	-2.6
89-12-48 5	5.3			-2.3		
84-12-60 4	6.5			-1.1		
CBV-CHL2			6.1			-4.6 ²
Average	6.1	4.3		-1.6	-1.9	-4.1

Sample	Mineral	Measured δD (‰)	$\delta\text{D}_{\text{fluid}}$ (‰)
89-12-48 5	Qtz	-148 ³	-148
84-12-60 4	Qtz	-171 ³	-171
CBV-CHL1	Chl	-102	-152 ²
CBV-CHL2	Chl	-112	-162 ²
Average			-158

1 Calculated using the equations of Matsuhisa et al (1979) for quartz, Friedman and O'Neil (1977) for calcite

2 Based on the empirical curves of Taylor (1979) at 280°C

3 Measured directly from crushed fluid inclusions

Shasta Electrum SEM Data

(semi-quantitative, Xray analyses)

Sample	grain	Au (at%)	Ag (at%)	Comment
JMPTHG-A	1	40.1	59.9	
	2	41.5	58.5	
	3	30.7	69.3	
	4a	41.1	58.9	core
	4b	38.3	61.7	core
	4c	19.1	80.9	rim
	4d	16.5	83.5	rim
JMPTHG-C	1	5.8	94.2	
	2	5.4	94.5	
	3	6.8	93.2	
	4	4.8	95.2	
	5a	41.3	58.7	core
	5b	10.5	89.5	rim
	6	43.8	56.2	
	7	9.5	90.5	
	8a	44.4	55.6	core
8b	9.7	90.3	rim	
<hr/>				
Average	All	24.1	75.9	
	Cores	41.3	58.7	
	Rims	13.9	86.1	

Shasta Sphalerite Probe Data

Sample	Comments	Weight Percent					Total %
		Zn %	Fe %	Cu %	Cd %	S %	
JMPT-HGD-1A		65.69	0.40	0.30	0.88	32.42	99.69
JMPT-HGD-1B		66.13	0.20	0.02	0.82	32.41	99.58
JMPT-HGD-2A		65.25	0.82	0.09	1.51	32.19	99.86
JMPT-HGD-2B		65.83	0.11	0.00	1.28	32.28	99.49
JMPT-HGD-3A		65.75	0.01	0.00	0.96	32.47	99.19
JMPT-HGD-3B		64.95	1.00	0.00	1.00	32.51	99.46
JMPT-HGD-3C		66.49	0.00	0.03	1.12	32.44	100.07
CB-VEIN-1A		65.09	1.01	0.15	0.55	32.93	99.73
CB-VEIN-1B		65.46	1.24	0.10	0.56	32.43	99.78
CB-VEIN-1C		65.24	1.02	0.14	0.57	32.57	99.53
Average (10)		65.59	0.58	0.08	0.92	32.46	99.64
Average (7)	JMPT-HGD	65.73	0.36	0.06	1.08	32.39	99.62
Average (3)	CB-VEIN	65.26	1.09	0.13	0.56	32.64	99.68

Sample	Comments						Stoichiometric Proportions (1 S atom)				
		Fe at. %	FeS mol %	FeS sample	XFe sp	XFe sample	Zn	Fe	Cu	Cd	S
JMPT-HGD-1A		0.35	0.696	0.636	0.007	0.006	0.99	0.01	0.00	0.01	1.00
JMPT-HGD-1B		0.18	0.358		0.004		1.00	0.00	0.00	0.01	1.00
JMPT-HGD-2A		0.72	1.423		0.014		0.99	0.01	0.00	0.01	1.00
JMPT-HGD-2B		0.10	0.199		0.002		1.00	0.00	0.00	0.01	1.00
JMPT-HGD-3A		0.01	0.020		0.000		0.99	0.00	0.00	0.01	1.00
JMPT-HGD-3B		0.88	1.754		0.018		0.98	0.02	0.00	0.01	1.00
JMPT-HGD-3C		0.00	0.000		0.000		1.01	0.00	0.00	0.01	1.00
CB-VEIN-1A		0.88	1.765	1.893	0.018	0.019	0.97	0.02	0.00	0.00	1.00
CB-VEIN-1B		1.08	2.141		0.022		0.99	0.02	0.00	0.00	1.00
CB-VEIN-1C		0.89	1.774		0.018		0.98	0.02	0.00	0.01	1.00
Average (10)		0.51	1.013		0.010		0.99	0.01	0.00	0.01	1.00
Average (7)	JMPT-HGD	0.32	0.636		0.006		1.00	0.01	0.00	0.01	1.00
Average (3)	CB-VEIN	0.95	1.894		0.019		0.98	0.02	0.00	0.00	1.00

Notes: Number in parentheses following average is number of analyses.

XFe=Fe/(Fe+Zn), based on atomic percent; mol % FeS in sphalerite.

Calculations for atomic % Fe, XFe and FeS are uncorrected for Cu, and thus do not account for possible chalcopyrite inclusions.

Lower detection limits 0.02-0.04 wt %; except 0.05 wt % for Zn.

Careca Camebax electron microprobe using PAP correction scheme; 20 kV, 20 nA, 25 s, 4 um beam.

Shasta Sphalerite Equilibria

Sample	Comments	XFe	T deg C	aS2 log	T deg C	aS2 log	T deg C	aS2 log
JMPT-HGD-1A		0.007	280	-9.3	250	-10.9	300	-8.3
JMPT-HGD-1B		0.004	280	-8.7	250	-10.3	300	-7.8
JMPT-HGD-2A		0.014	280	-9.9	250	-11.5	300	-9.0
JMPT-HGD-2B		0.002	280	-8.2	250	-9.8	300	-7.3
JMPT-HGD-3A		0.000	280	-6.2	250	-7.8	300	-5.3
JMPT-HGD-3B		0.018	280	-10.1	250	-11.7	300	-9.1
JMPT-HGD-3C		0.000	280	ERR	250	ERR	300	ERR
CB-VEIN-1A		0.018	280	-10.1	250	-11.7	300	-9.2
CB-VEIN-1B		0.022	280	-10.3	250	-11.9	300	-9.3
CB-VEIN-1C		0.018	280	-10.1	250	-11.7	300	-9.2
Average (10)		0.010	280	-9.6	250	-11.2	300	-8.7
Average (7)	JMPT-HGD	0.006	280	-9.2	250	-10.8	300	-8.3
Average (3)	CB-VEIN	0.019	280	-10.2	250	-11.8	300	-9.2

Notes: S2 activities calculated assuming divariant assemblage of sphalerite-pyrite.
 aS2 calculated using equation of Barton and Skinner (1979); if equation of Scott and Barnes (1971) is used, aS2 would be 0.4 log units lower at 280 deg C, 0.5 log units lower at 250 deg C, and 0.3 log units lower at 300 deg C.

Shasta Chlorite Probe Data

Sample	Comments	Weight Percent							Total %
		SiO ₂ %	TiO ₂ %	Al ₂ O ₃ %	FeO %	MnO %	MgO %	CaO %	
87-32-40.2-1A	vein margin	27.38	0.01	19.70	15.98	4.53	19.30	0.07	86.98
87-32-40.2-1B	vein margin	27.94	0.01	19.89	15.76	3.28	21.74	0.06	88.66
8-2-114.2-1A	vein margin	25.38	0.01	19.34	23.70	2.89	14.58	0.03	85.94
8-2-114.2-1B	vein margin	25.66	0.03	20.04	24.55	2.66	14.35	0.08	87.37
8-2-114.2-1C	vein margin	26.09	0.00	19.77	23.97	3.07	15.04	0.07	88.01
8-2-114.2-2A	vein margin	26.20	0.00	19.79	22.27	3.19	15.84	0.04	87.32
8-2-114.2-2B	vein margin	26.22	0.03	19.60	21.62	2.59	16.97	0.07	87.09
87-23-40.2-2A	vein	30.15	0.01	16.60	16.47	1.37	23.09	0.10	87.79
87-32-40.2-2B	vein	29.50	0.01	17.46	16.12	1.70	22.40	0.11	87.30
89-11-39.5-2A	vein	30.42	0.02	20.70	13.74	4.28	18.05	0.13	87.33
89-11-26.0-1A	vein	31.50	0.03	19.90	13.09	1.94	21.30	0.12	87.88
89-11-26.0-1B	vein	29.86	0.01	19.00	13.23	1.13	23.78	0.08	87.10
89-11-26.0-2A	vein	28.36	0.01	20.61	14.22	2.74	21.02	0.14	87.10
Average (7)	vein margin	26.41	0.01	19.73	21.12	3.17	16.83	0.06	87.34
Average (6)	vein	29.96	0.02	19.05	14.48	2.19	21.61	0.11	87.42

Shasta Chlorite Probe Data, Cont'd

Sample	Comments	Stoichiometric Proportions (28 O)									
		Si	Aliv	sumZ	Alvi	Ti	Fe	Mn	Mg	Ca	sumY
87-32-40.2-1A	vein margin	5.976	2.024	8.00	3.044	0.001	1.312	0.838	6.277	0.017	11.49
87-32-40.2-1B	vein margin	5.917	2.083	8.00	2.881	0.001	1.256	0.588	6.861	0.014	11.60
8-2-114.2-1A	vein margin	6.017	1.983	8.00	3.421	0.002	2.113	0.580	5.153	0.009	11.28
8-2-114.2-1B	vein margin	6.000	2.000	8.00	3.521	0.005	2.160	0.527	5.001	0.021	11.23
8-2-114.2-1C	vein margin	6.025	1.975	8.00	3.405	0.001	2.082	0.601	5.177	0.018	11.28
8-2-114.2-2A	vein margin	6.007	1.993	8.00	3.355	0.000	1.922	0.619	5.414	0.010	11.32
8-2-114.2-2B	vein margin	5.979	2.021	8.00	3.244	0.004	1.855	0.499	5.765	0.016	11.38
87-23-40.2-2A	vein	6.418	1.582	8.00	2.583	0.002	1.319	0.247	7.324	0.023	11.50
87-32-40.2-2B	vein	6.310	1.690	8.00	2.712	0.002	1.298	0.308	7.142	0.025	11.49
89-11-39.5-2A	vein	6.390	1.610	8.00	3.515	0.003	1.086	0.761	5.650	0.029	11.04
89-11-26.0-1A	vein	6.453	1.547	8.00	3.259	0.004	1.009	0.337	6.504	0.027	11.14
89-11-26.0-1B	vein	6.202	1.798	8.00	2.854	0.002	1.034	0.199	7.363	0.018	11.47
89-11-26.0-2A	vein	6.001	1.999	8.00	3.141	0.002	1.132	0.490	6.630	0.031	11.43
Average (7)	vein margin	5.987	2.013	8.00	3.260	0.002	1.802	0.609	5.687	0.015	11.37
Average (6)	vein	6.296	1.704	8.00	3.013	0.003	1.145	0.390	6.767	0.026	11.34

Notes: Remainder of weight totals assumed to be H₂O. O by stoichiometry; total Fe as FeO.

Number in brackets following average is number of analyses.

Lower detection limits 0.02-0.03 wt %, except 0.04-0.05 wt % for MgO and FeO. Precision for Al₂O₃ estimated at +/-1 % relative to measured values. Cameca Camebax electron microprobe using PAP correction scheme; 20 nA, 15 kV, 25 s, 4 um beam.

Shasta Chlorite Geothermometry

Sample	Comments	Aliv	T deg C
87-32-40.2-1A	vein margin	1.012	264
87-32-40.2-1B	vein margin	1.042	273
8-2-114.2-1A	vein margin	0.991	257
8-2-114.2-1B	vein margin	1.000	260
8-2-114.2-1C	vein margin	0.988	256
8-2-114.2-2A	vein margin	0.996	259
8-2-114.2-2B	vein margin	1.011	263
87-23-40.2-2A	vein	0.791	193
87-32-40.2-2B	vein	0.845	210
89-11-39.5-2A	vein	0.805	197
89-11-26.0-1A	vein	0.773	187
89-11-26.0-1B	vein	0.899	227
89-11-26.0-2A	vein	0.999	260
Average (7)	vein margin	1.006	262
Average (6)	vein	0.852	212

Notes: Aliv is stoichiometric proportion of tetrahedral aluminum, based on 14 O (half cell; see table of chlorite data).
Temperatures calculated using the empirical relationship between site occupancy and T as described by Cathelineau (1988).
Error based on analytical uncertainty of probe data alone is +/-3 deg C.

Shasta Acanthite Probe Data

Sample	Comments	Weight Percent									
		Au %	Ag %	Cu %	Fe %	Zn %	Hg %	Bi %	Cd %	S %	Total %
JMPT-HGD-1A		0.01	86.12	0.19	0.03	0.00	0.02	0.00	0.00	13.34	99.70
JMPT-HGD-1B		0.00	85.97	0.27	0.01	0.00	0.00	0.04	0.00	13.41	99.69
JMPT-HGD-1C		0.00	86.02	0.18	0.04	0.02	0.03	0.02	0.00	13.82	100.12
Average (3)		0.00	86.04	0.21	0.03	0.01	0.01	0.02	0.00	13.52	99.84

Sample	Comments	Stoichiometric Proportions (1 S atom)								
		Au	Ag	Cu	Fe	Zn	Hg	Bi	Cd	S
JMPT-HGD-1A		0.00	1.92	0.01	0.00	0.00	0.00	0.00	0.00	1.00
JMPT-HGD-1B		0.00	1.91	0.01	0.00	0.00	0.00	0.00	0.00	1.00
JMPT-HGD-1C		0.00	1.85	0.01	0.00	0.00	0.00	0.00	0.00	1.00
Average (3)		0.00	1.89	0.01	0.00	0.00	0.00	0.00	0.00	1.00

Notes: Number in parentheses following average is number of analyses.

Lower detection limits 0.02-0.06 wt %; except 0.08 wt % for Au and Bi, 0.09 for Hg and 0.10 wt % for Cd.
 Cameca Camebax electron microprobe using PAP correction scheme; 20 kV, 20 nA, 25 s, 4 μ m beam.

Shasta Electrum/Silver Probe Data

Sample	Comments	Weight Percent									
		Au %	Ag %	Cu %	Fe %	Zn %	Hg %	Bi %	Cd %	S %	Total %
JMPT-HGD-1C		0.00	99.21	0.05	0.02	0.02	0.02	0.03	0.00	0.03	99.37
JMPT-HGD-1D		0.03	99.88	0.00	0.00	0.00	0.00	0.00	0.00	0.05	99.96
JMPT-HGD-1E		2.48	97.52	0.07	0.01	0.05	0.06	0.06	0.00	0.11	100.36
JMPT-HGD-3A		0.00	99.45	0.04	0.05	0.02	0.02	0.00	0.00	0.08	99.65
Average (4)		0.63	99.02	0.04	0.02	0.02	0.02	0.02	0.00	0.07	99.84

Sample	Comments	Atomic Percent											
		Ag: Au	XAg	XAg sample	Au	Ag	Cu	Fe	Zn	Hg	Bi	Cd	S
JMPT-HGD-1C		0.000	1.00	1.00	0.00	99.70	0.08	0.04	0.04	0.01	0.01	0.00	0.12
JMPT-HGD-1D		0.000	1.00		0.02	99.82	0.00	0.00	0.00	0.00	0.00	0.00	0.16
JMPT-HGD-1E		0.025	0.99		1.37	97.99	0.11	0.03	0.08	0.03	0.03	0.00	0.35
JMPT-HGD-3A		0.000	1.00		0.00	99.55	0.06	0.09	0.03	0.01	0.00	0.00	0.26
Average (4)		0.006	1.00		0.35	99.27	0.06	0.04	0.04	0.01	0.01	0.00	0.22

Notes: Number in parentheses following average is number of analyses.

XAg=Ag/(Ag+Au), and average values also given each sample; Ag: Au is weight ratio.

Lower detection limits 0.04-0.09 wt %; except 0.10 wt % for Hg and Cd, 0.03 for Fe, and 0.01 wt % for S.

Cameca Camebax electron microprobe using PAP correction scheme; 20 kV, 20 nA, 25 s, 4 μm beam.

Shasta Carbonate Probe Data

Sample	Comments	XC03				Weight Percent				
		FeCO3 mol %	MgCO3 mol %	CaCO3 mol %	MnCO3 mol %	FeO %	MgO %	CaO %	MnO %	Total %
87-32-40.2-2A		0.20	0.05	95.99	3.76	0.13	0.03	53.37	2.64	56.17
87-32-40.2-2B		0.00	0.00	98.47	1.53	0.01	0.00	54.16	1.06	55.22
87-32-40.2-2C		0.00	0.00	97.40	2.60	0.01	0.00	53.58	1.80	55.39
87-32-40.2-2D		0.00	0.00	97.06	2.94	0.00	0.00	53.60	2.05	55.65
Average (4)	late, mineralized vein carb	0.05	0.01	97.22	2.71	0.03	0.01	53.68	1.89	55.61

Notes: 0 by stoichiometry; remainder of weight totals assumed to be CO2. Total Fe as FeO.
 Number in brackets following average is number of analyses.
 Lower detection limits 0.04-0.07 wt %; except 0.02 wt % for MgO.
 Cameca Camebax electron microprobe using PAP correction scheme; 15 nA, 10 kV, 25 s, 7 um beam.